2009

Subcellular localization of NEDD9 and HMB45 with AQUA technology to distinguish Spitz nevi from melanoma

Matthew C. McRae
Yale University

SUBCELLULAR LOCALIZATION OF NEDD9 AND HMB45 WITH AQUA TECHNOLOGY TO DESTINGUISH SPITZ NEVI FROM MELANOMA

A Thesis Submitted to the

Yale University School of Medicine

In Partial Fulfillment of the Requirements for the

Degree of Doctor of Medicine and

Degree of Masters in Health Science Research

By

Matthew C. McRae

2009

Abstract

SUBCELLULAR LOCALIZATION OF NEDD9 AND HMB45 WITH AQUA TECHNOLOGY TO DISTINGUISH SPITZ NEVI FROM MELANOMA.

Matthew C. McRae, Rossitza Lasova, Bonnie Gould-Rothberg, David Rimm (Sponsored by Deepak Narayan). Section of Plastic Surgery, Department of Surgery, Yale University School of Medicine, New Haven, CT.

Our hypothesis is that the expression level and subcellular localization of HMB45 and NEDD9 as demonstrated by the ln(nuclear/non-nuclear) Automated Quantitative Analysis (AQUA) score, defined as the subcellular AQUA ratio, will be consistently altered between benign nevi and melanoma and between Spitz nevi and Spitzoid melanoma. Our specific aims are to assess quantitative expression and subcellular localization of HMB45 and NEDD9 to aid in the diagnosis of benign Spitz nevi and malignant Spitzoid melanoma. This remains a vexing clinical problem with important implications for treatment and patient care. The quantitative expression and subcellular AQUA ratio will be assessed in the following samples: benign derived versus malignant derived cell lines, human benign nevi, human primary melanoma, human metastatic melanoma, typical Spitz nevi, atypical Spitz nevi and Spitzoid melanoma. AQUA was used to quantify protein expression levels in subcellular compartments using fluorescence-based immunohistochemistry. Tissue Microarrays (TMA) analysis was used for cell line, benign nevi and malignant melanoma while whole section analysis was used for Spitz nevi and Spitzoid melanoma. NEDD9 subcellular AQUA ratio was significantly reduced in primary melanoma (mean=-0.645, std dev=0.29) versus benign nevi (mean =

-0.429, std dev=0.108) on YTMA98-2 ($p=0.0086$), significantly reduced in melanoma metastases (mean=-0.482, std dev=0.149) versus benign nevi (mean= -0.342, std dev=0.159) on YTMA66A ($p<0.0001$), and significantly reduced in primary melanoma (mean= -0.435, std. dev.=0.185) and melanoma metastases (mean= -0.42, std. dev.= 0.188) versus benign nevi (mean= -0.319, std. dev.= 0.141) in SPORE84 array ($p=0.0003$, Tukey/Kramer post-hoc significance $p<0.05$). HMB45 subcellular AQUA ratio was significantly reduced in primary melanoma (mean=-0.463, std. dev.=0.264) versus benign nevi (mean=-0.159, std. dev.=0.158) on YTMA 98-2 array ($p=0.0001$). On whole section analysis, the HMB45 and NEDD9 subcellular AQUA ratio shared a similar distribution between Spitz nevi, atypical Spitz nevi and Spitzoid melanoma. Subcellular localization using the subcellular AQUA ratio of HMB45 and NEDD9 defines benign nevi from melanoma on TMA but is not useful in discriminating between benign Spitz nevi and melanoma with Spitzoid features. The maximum HMB45 AQUA score in the tumor mask in a single 20X high-powered field of a whole tissue section was deemed promising on discovery analysis at differentiating between Spitz nevi and melanoma with Spitzoid features ($p=0.007$, receiver operating characteristic area under curve 0.711) but requires validation on an independent cohort.

Acknowledgements

Thank you to the Yale School of Medicine Office of Student Research. My research career began in the first year of medical school with the intensive pedagogical experience in Bar Harbor, Maine. This experience kindled in me an interest that has already had a profound impact on my career. This started a cascade of events leading to a year of dedicated research funded by the generous support of the Doris Duke Clinical Research foundation. Thank you to Dr. John Forrest, Donna Carranzo and Mae Geter for your support in making so many opportunities available to me for development as a physician and scientist.

Thank you to the greatest family on earth. My parents Susan and John whose daily conversations keep me grounded, brother Peter and sister Amy whose NYC apartment is a piece of home and twin brother Mark - “from the womb to the tomb”.

Thank you to Dr. David Rimm whose absolute brilliance as both scientist and manager kept me both inspired and on task. As a gifted scientist, teacher, clinician and athlete, Dr. Rimm is the triple threat and one. It was a privilege to work with cutting edge laboratory technology with direct implications for improving patient care. From lab meeting to journal club and weekly progress meetings, the lessons learned in the Rimm laboratory are gifts that I will always value and put to good use.

Thank you to Dr. John Geibel and Dr. Rossitza Lasova for agreeing to be members of my thesis committee and for your guidance and support over the course of the year.

Thank you to Jason Hanna as the man who always took time out of his day to explain everything from experimental protocols to the intricacies of how to pipette. Thank you to Jen Bordeaux and Seema Agarwal for your insight into the world of cell biology and the greater world at large. Thank you to Veronique for your introduction to AQUA technology and scooters. Thank you to lab managers Elizabeth Killiam and Chris Moeder for your daily help and camaraderie. Thank you to Maria Baquero for your help with working with whole sections and data organization. Thank you to Dr. Bonnie Rothberg, the captain of team melanoma, for your oversight and support. Thank you to Elsa Anagnostou for your help with data analysis, experimental-protocols, and for always being there when I needed help.

Finally thank you to Dr. Deepak Narayan. Beyond my immediate family, there is no one I trust so completely to have my best interest at heart. You have opened the world of plastic surgery to me through research, national meetings and clinical care both in this country and as far abroad as Thailand. You are the complete mentor and I know that I can always count on you. I am so grateful.

TABLE OF CONTENTS

Introduction

Melanocytes, Nevi and Melanoma

Melanocytes are derived from the neural crest in embryogenesis and migrate throughout the body to the eye, ear, leptomeninges and particularly to the basal layer of the epidermis. The lowest concentration of melanocytes in the epidermal basal layer is found in the skin of the trunk and upper arm with 800 to1000 per square millimeter (roughly one melanocyte per ten keratinocytes) while the highest concentration is found on the face and genitalia with over 2000 melanocytes present per millimeter of skin (roughly one melanocyte per four keratinocytes)[1]. The total melanocyte mass in the body is thought to range between 1 and 1.5 mL^2. The difference in skin tone between human beings is a result of the basal activity level of melanocytes instead of relative number of cells as the relative concentration of melanocytes is independent of race and sex [3].

Melanocytes transfer melanosomes to surrounding keratinocytes to protect their nuclei from ultra-violet radiation. Freckles or lentigo result from isolated clusters of heavily pigmented keratinocytes. In contrast, acquired nevi are a benign neoplasm or hamartoma of melanocytes that have overcome contact inhibition to form nests of cells in response to inciting factor such as UV light[4]. If present at birth, nevi are congenital and are thought to be a result of an error in development and migration of neural crest elements arising from the dermis into the epidermis [5].

Congenital nevi occur in 1-3% of the population. From birth, there is an increasing number of acquired nevi that peak in late adolescence[6]. The majority of fair skinned individuals have several nevi. Nevi can be defined by their location in the cutis. Nevi are junctional if located at the border of the dermis and epidermis, intradermal if located entirely in the dermis and compound if located both in the dermis and epidermis.

Nevi are recognized as a benign neoplasm with little to no chance of progression to malignancy. A group of researchers at Massachusetts General Hospital quantified the lifetime risk by age 80 of malignant transformation of any nevi greater than 3mm into cutaneous melanoma as 0.03% for men and 0.009% for women[7]. Certain variants of nevi are thought to have greater malignant potential over the course of a lifetime necessitating removal or close observation. Dysplastic nevi when associated with dysplastic nevi syndrome are at a greater risk of malignant transformation. Large (1-3cm) or giant (>3cm) congenital nevi have a lifetime incidence of malignant transformation of around 5% although literature reviews report the incidence as being somewhere between 0 and 42%[8].

Melanoma is the malignant transformation of melanocytes causing cancer. Although melanoma is the leading cause of skin cancer-related deaths worldwide, it accounts for only 4% of all skin cancers. The American Cancer Association estimates that 62,480 new melanomas were diagnosed in 2008 with 8420 deaths resulting from the disease. For Caucasians, 1 in 50 will get melanoma for a lifetime incidence of 2%. Hispanics and Blacks have far lower lifetime risk of 0.5% and 0.1 % respectively. Risk factors for acquiring melanoma include exposure to UV light resulting in severe burns, multiple dysplastic nevi, personal or family history of melanoma, increasing age,

immunosupression, fair skin and xeroderma pigmentosum. Men have a slightly higher incidence of melanoma with higher melanoma related mortality[9].

Spitz Nevi

Sophie Spitz reported on a series of childhood melanocyte lesions with histological features of melanoma that behaved in a benign manner[10]. She reported on a juvenile variant of cutaneous melanoma composed of spindle or epithelioid melanocytes in which the prognosis was excellent. Subsequent studies revealed "Spitz" nevi as benign. Classic and atypical Spitz nevi are an uncommonly occurring lesion of melanocytes with an incidence of 7 in 100,000[11]. They generally appear in the head and neck region or the lower extremities of a child as a pink papule but they can also be heavily pigmented. They derive either from pre-existent nevi or arise *de novo* and rapidly grow to a size of around 1cm at which point they often become quiescent. Incomplete removal can result in recurrence.

Spitz nevi most commonly present in children and adolescents but may also occur in adults. 50% occur by age 10 and 70% occur by age 20. A study completed at Yale University reported on the incidence of Spitz Nevi according to age and showed that the ratio of Spitz Nevi to melanoma varies with age. In those younger than 20 years of age the ratio of Spitz nevi to melanoma is 60 to 1. In people over age 50, the ratio of Spitz nevi to melanoma is 1 to 60.[12]

Despite greater than 60 years of study, there remains no consensus among dermatopathologists on which criteria define a Spitz nevus. The diagnosis of Spitz nevi is

reliant on more than just the clinical history and macroscopic appearance of the lesion. Commonly found pathologic features of Spitz nevi fall into major and minor histological criteria and are summarized below:

Table 1: Criteria Used for Establishing Diagnosis of Spitz Nevi. Adapted from Crotty *et al.* and Dahlstrom *et al*[13, 14].

Major Criteria	Minor Criteria
Symmetry and well circumscribed lateral margins. Lack of lateral extension of junctional nevus cells beyond dermal nevus cells. Epithelioid and/or spindle cells. Spindle cells are more common. Cells arranged in fascicles with vertical orientation related to the rete ridges. Maturation of the deep dermal component of the nevus. This means that nevus cells in the deeper part of the lesion are smaller and become dispersed among reticular dermal fibers with progressive descent into the dermis. Kamino Bodies, which are eosinophilic globules. Pagetoid (or upward) spread that is only focal and limited to the lower portion of the epidermis.	Junctional cleavage Absence of nuclear pleomorphism Superficial Multinucleated Giant Cells Hyperkeratosis and acanthosis of the epidermis No deep or atypical mitosis (mitosis may be present in the junctional or superficial dermal components) Superficial edema, telangiectasia, perivascular inflammation
NB: Most Spitz nevi do not display all of these characteristics	

Atypical Spitz nevi display features that are not sufficient for a diagnosis of melanoma. However, neither the number nor degree of atypical features for a diagnosis of atypical Spitz nevi has ever been defined. As a result, what may be deemed atypical

Spitz in an adult will be classified as classic Spitz in a child. Atypical features that classify Spitz nevi as low or high risk are listed below:

Table 2: Atypical features of Spitz Nevi useful in classifying as low or high risk of malignancy. Adapted from Barnhill *et al*[15].

Low Risk	High Risk
<10 years old	>10 years old
No ulceration	Ulceration
Small size (<10 mm)	Large size (>10 mm)
Symmetry	Asymmetry
Superficial only	Deep extension (into sub cutis)
Less cellularity	Hypercellularity
Maturation	No maturation
Minimal or low grade cytological atypia	Prominent cytological atypia
Few or no mitoses	Prominent mitotic rate
Superficial mitoses only	Deep mitoses
Typical mitoses	Atypical mitoses

For between 80 and 90% of Spitz lesions, the diagnosis is clear[11]. However for the remaining lesions, there are clinical and histological features of melanoma. Spitzoid melanoma is the variant of melanoma that shares clinical features with Spitz nevi. There is no single discriminating factor between Spitz nevi and malignant melanoma as every trait of Spitz nevi has been described in melanoma[11]. The current criteria used to

distinguish benign Spitz nevi from melanoma with Spitzoid features are delineated below:

Table 3: Features in Favor of Spitz nevi versus Spitzoid Melanoma. Adapted from Crotty *et al.*[14]

Features of Spitz Nevi	Features of Spitzoid Melanoma
Kamino Bodies Symmetry Uniformity of nests across lesion	Dermal mitotic rate >2/mm^2 Mitosis within 0.25 mm of the tumor base Atypical mitoses

While Spitz nevi most commonly occur in children - a population where melanoma is quite rare - it is estimated that 40% of children who do develop melanoma are originally misdiagnosed[16,17]. As melanoma is on the differential of every Spitz nevus, differentiating between the two is incredibly important in terms of treatment (Figure1).

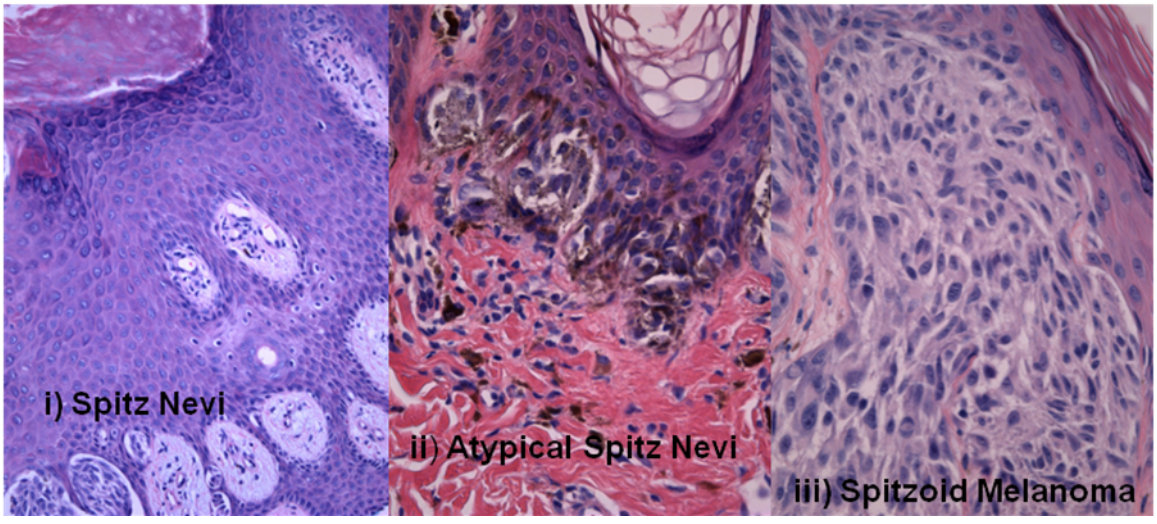

Figure 1: H+E slides of i) typical Spitz Nevi ii) atypical Spitz Nevi and iii) Spitzoid Melanoma. Differentiating between these tumor types can be a challenge and while typical and atypical Spitz are benign, malignant melanoma is potentially life threatening.

The treatment of Spitz nevi consists of surgical excision with margins of 0.5cm. If the lesion is deemed melanoma, surgical margins of up to 2 cm will be necessary as well as sentinel node biopsy and the potential for additional immune therapy. Since Spitz nevi tend to occur in the head and neck region of young children, treatment of Spitz nevi as a melanoma can result in unnecessary morbidity from removal of larger margins of healthy tissue while under-treatment of melanoma can result in premature death. There are also medico-legal consequences of this difficult diagnosis for pathologists. A study investigating all malpractice claims in Napa Valley between 1998 and 2003 found that a false negative melanoma diagnosis was the single most common reason for malpractice claims against a pathologist and nearly one third of these claims involved misdiagnosis as Spitz nevi, dysplastic nevi, spindle-cell, squamous cell, atypical fibroxanthoma, and dermatofibroma[18].

Molecular Pathology Part1: HMB45

Human Melanoma Black-45 (HMB-45) is a monoclonal antibody that recognizes the glycosylated form of gp100 protein[19]. Gp100 or Pmel17 is the human homolog of the mouse silver protein. It is required for the proper formation of melanosomal fibrils, which facilitates the maturation of stage I premalanosomes to stage II and is restricted to the fibrillar matrix of stage II premelanosomes[20, 21].

HMB45 is used for the identification of melanoma cells in sentinel lymph nodes. Malignant melanoma reacts positively with HMB45 antibody in most cases with the

exception of desmoplastic and spindle cell types[22]. Junctional nevi and the epidermal component of compound nevi generally stain positively for HMB45 while the dermal component of compound nevi usually stain negatively. The HMB45 antibody in dysplastic nevi has been shown to stain positively in both the epidermal and dermal components [23]. In a study that compared the HMB45 staining pattern of typical Spitz nevi, compound nevi and melanoma, it was shown that while 100% of the 12 melanoma had both epidermal and dermal staining to the base of the lesion, only 2 of 17 Spitz nevi and 0 of 20 compound nevi had similar staining[24].

The nuclear localization of gp100 was not appreciated until recently due to the limits of chromogenic staining and presence of the overwhelming hematoxylin counter-stain on the nucleus. Gould-Rothberg *et al.* demonstrated that fluorescence based immunohistochemistry signaling enabled the discovery of differential subcellular staining patterns between benign nevi and malignant cells with notable HMB-45 staining in the nucleus of benign nevi. The ln(nuclear/non nuclear) AQUA ratio of HMB45 staining maximized the contrast of predominantly nuclear staining benign in nevi versus the predominantly cytoplasmic staining in malignant melanoma lesions with an odds ratio of 2.24. While the cases were selected from several institutions as classic examples of the histotype, a maximized sensitivity of 0.92 and specificity of 0.80 suggests the potential utility of this ratio as a diagnostic tool in the characterization of melanocytic lesions[20]. The subcellular localization and AQUA ratio of gp100 as revealed by HMB45 fluorescent immunostaining has yet to be characterized in Spitz nevi, representing a potential histological discriminator between the cell types.

Molecular Pathology Part2: NEDD9

Neural precursor cell Expressed Developmentally regulated expression pattern in brain 9 (NEDD9) was identified in 2006 as a melanoma metastasis gene by comparative oncogenomics. The gene was localized to chromosome 13A3.3 in mice with the corresponding human homologue at 6p25-24. A group from Harvard demonstrated over expression of Nedd9 in metastatic melanoma relative to primary melanoma. They showed Nedd9 as having a role in focal adhesion contacts in the cell periphery suggesting a mechanism of metastasis and invasion, as well as showing enhanced invasion *in vitro* and metastasis *in vivo* of both normal and transformed melanocytes. The staining pattern on formalin fixed, paraffin embedded tissue was described as "patchy" in nevi (n=31), versus "strong broad over expression" in primary and metastatic melanoma (n=40), correlating with melanoma progression. Scores were calculated on a 0 to 4 categorical scale and arrived at by consensus evaluation by pathologists[25].

It has been recently shown that mesenchymal type movement of melanoma cells are driven by a GTPase. This GTPase is activated through a complex containing Nedd9 [26]. Nedd9 has also been implicated in glioblastoma multiforme invasion[26], and is up regulated in lung cancer metastasis [27].

Preliminary data in the Rimm laboratory suggest that Nedd9 shares the propensity for nuclear expression in the benign nevi while cytoplasmic/membranous expression occurs in both primary and metastatic melanoma.

Tissue Microarrays and Automated Quantitative Analysis

Tissue microarrays (TMA) permit the analysis of large cohorts of patients simultaneously, thus providing a high throughput method of analyzing both the prognostic and diagnostic utility of protein targets [28]. Although several protein biomarkers may be targeted in a single experiment, TMAs are generally used for the analysis of a single target of interest but in a high throughput fashion. Putting samples on the same slide and staining under identical experimental conditions permit a reproducible method of analyzing molecular protein expression. The assay used to detect antigens in tissue with fluorescence-linked antibodies is known as immunohistochemistry (IHC). TMAs may be used for other experimental platforms as well including DNA alterations with fluorescence *in situ* hybridization and mRNA expression by *in situ* hybridization.

Automated subcellular localization and quantification of protein expression in tissue microarrays or AQUA™ (HistoRX, New Haven, CT) is image analysis software that permits the rapid, automated, continuous and quantitative analysis of tissue microarrays and tissue whole section including the subcellular localization of signal and separation of tumor from stroma[29]. Continuous, quantitative scoring is not possible with chromogen based IHC protocols that requires a pathologist to rely on the subjective discernment of the naked eye. Many conditions can influence their judgment of intensity of staining including background staining, stromal staining and even the order in which the slide is observed [28]. AQUA results in scores that are directly proportional to protein molecules per cell. This is accomplished by incorporation of standard curves resulting from cell lines present within TMA cores and can therefore serve as a mechanism of determining the tissue concentration of the protein *in situ.*

Hypothesis

The expression level and subcellular localization of HMB45 and NEDD9 as defined by ln(nuclear/non-nuclear) AQUA score have been show to be consistently altered between benign nevi and melanoma. Here we hypothesize that this test could be useful in discriminating between benign Spitz nevi and Spitzoid melanoma.

Specific Aims of Thesis

Aim 1

Assess expression levels and subcellular localization of HMB45 and NEDD9 in benign derived versus malignant derived cell lines to validate antibodies.

Aim 2

Assess quantitative expression levels and subcellular AQUA ratio of HMB45 and NEDD9 in human benign nevi, human primary melanoma and human metastatic melanoma.

Aim 3

Assess quantitative expression levels and subcellular AQUA ratio of HMB45 and NEDD9 in typical Spitz nevi, atypical Spitz nevi and Spitzoid melanoma in order to determine the clinical utility of the HMB45 and NEDD9 biomarkers.

Methods

Melanoma Tissue Microarray:

(*Lori Charette of the Yale tissue microarray facility completed TMA preparation. The SPORE 84 array was provided by a peer institution*). TMAs were constructed using the standard method [30]. After tumor was removed from the patient, it was fixed in formalin, embedded in paraffin and archived. Tumor types were searched for and retrieved to form the cohort. 600-micron diameter cores from representative sections of tumor were then taken using a precision arraying instrument (Beecher Instruments, Silver Spring, MD) to form a "master block." The cores were spaced 800 microns apart in the master block (600 or more tissue cores can be placed in a single master block that can then be sectioned to produce between 100 and 200 slides for simultaneous cohort analysis). Often cell line controls were placed on the tissue microarray for both internal and external validation of experimental procedure. Cell line pellets were made after growing cell lines to confluence. This was followed by 10% formalin fixation and embedding in paraffin. 0.6 mm cores were then made for inclusion in the master block and subsequently sectioned.

Using an ultraviolet light cross-linking transfer system the 5-micrometer thick sections were fastened to the adhesive slide (Instrumedics Inc., Hackensack, NJ) and dipped in paraffin for storage. Every 10th slide was stained with hematoxylin and eosin (H&E) and reviewed by a pathologist to confirm the diagnosis. During staining, an internal reviewer (*Matthew McRae*) observed all histospots. Generally, TMA slides were

cut for immediate use. If slides were not used immediately, they were place in a nitrogen desiccation chamber to prevent antigen oxidation and breakdown.

For our study, we used four different tissue micro-arrays: the Yale melanoma test arrays, the Yale Boutique tissue microarray 98-2, the Yale Nevi Array 66A, and the Specialized Program Of Research Excellence (SPORE) Melanoma Progression Array 84.

Yale melanoma test array: A variety of test arrays were used for titering of antibodies to achieve ideal dilutions, and for negative control during experiments (a negative control is when no primary target antibody is placed on the TMA during an experiment). Yale Tissue Microarray (YTMA) 112 has 10 melanoma metastases, 10 primary melanomas, 10 nevi, 6 normal skin and 4 cell lines. YTMA 109 has 10 melanoma metastases, 10 primary melanomas, 5 benign nevi, and 5 normal skin spots.

Yale Boutique TMA 98-2: This TMA was constructed out of formalin-fixed, paraffin embedded archived material by the Yale tissue microarray facility. The cohort includes 20 benign nevi, 20 vertical growth phase primary melanomas, and 20 metastases from subcutaneous, lymph node and visceral sites. Cell lines were included in duplicate on the array for a total of 90 cell line spots. The 24 melanoma cell lines present were 928, mel888, mm127, 501, BHP 18-21, yusac2, yumor, mel624, sk23, Aaron1, 1335, yumac, yugen8, 1241, mnt1, yusit1, yuheikp16, yurifp5, yuficp8, yulacp8, ww165, malme314, skmel, skmel28. The 21 non-melanoma cells included were IMR32, CHP212, ACL-a, SW480, HT29, CACO2, SKOV3, A431, MB231, T47D, MB435, ZR751-B, SKBR-3-A, MCF7, A549, NCI-H28, H1666, H1819, H2126, H2882, ANH1299.

Yale Nevi Array 66A: Dr. Harriet Kluger and the Yale tissue microarray facility

constructed this TMA out of formalin-fixed, paraffin-embedded archived material. The cohort included 299 benign nevi, 40 melanoma metastases, 13 normal skin, and 28 spots for 14 melanoma cell lines allowing for a two fold redundant internal control. These melanoma cell lines are YUSAC2, YUMOR, MEL624, SK23, 928, MEL888, 501, YUSIT, MNT1, 1241, YUGEN8, AARON, 1335.

SPORE Melanoma Progression Array 84: This TMA was constructed from archived formalin-fixed, paraffin embedded tissue from MD Anderson Cancer center, the University of Pennsylvania, and Harvard University. The array includes 21 thin nevi of under 1mm, 15 thick nevi of greater than 1mm, 38 radial growth phase primary melanomas, 20 vertical growth phase primary melanomas, 28 lymph node metastases and 45 visceral organ metastases. Thin lesions and metastases had duplicate cores on the array. Thick lesions had 3 cores from superficial, mid level and deep parts of the lesion. Duplicate cores were taken at each depth for all thick tumors.

Antibody Validation:

HMB45: The HMB45 mouse monoclonal IgG (Biogenex, San Ramon California) antibody has been used extensively and validated in the Rimm laboratory over several years by Bonnie Rothberg and Christopher Moeder.[20] They determined that the ideal titer of antibody was predilute HMB45 mouse monoclonal IgG (Biogenex, AM001-5M, clone HMB45, San Ramon California). A new aliquot of antibody necessitated titering of antibodies on YTMA109 test array at predilute, 1:50, 1:100, 1:500, 1:1000, and 1:5000. When an ideal concentration was arrived at, staining was completed on the YTMA 98-2

Boutique array. (*HMB45 antibody validated by Bonnie Gould-Rothberg and William Bradley. Validation on YTMA98-2 by Matthew McRae)*

Nedd9: Nedd 9/HEF1 mouse monoclonal IgG (Abcam, 18056, clone 2G9, Burlingame, CA) antibody was used based on previous work in the Rimm laboratory suggesting that the ideal concentration for paraffin embedded tissue was at 1:500. Immunohistochemically stained melanoma test arrays at 1:50, 1:100, 1:500, 1:1000, 1:5000 (three orders of magnitude) were analyzed with AQUA. With the ideal titer arrived at through analysis of signal to background, the YTMA98-2 Boutique array was stained and analyzed with AQUA for cell lines validation. Western blot analysis was then executed on cell line lysate to assure that staining was representative of the protein of interest. Finally Western blot of cultured human foreskin melanocytes provided by the laboratory of Ruth Halaban and cultured by Antonella Bacchiocchi was used to verify Nedd9 protein expression in benign melanocytes. This was used as a proxy to verify Nedd9 staining in benign nevi.

The protocol for Western blots was described previously in our laboratory[31]. The primary antibody was Nedd9 (Abcam, 18056, clone 2G9, Burlingame CA) at 1:2000. The secondary antibody was goat anti-mouse HRP conjugated (Santa Cruz Biotechnology, Santa Cruz CA). The detection system used was SuperSignal West Pico chemiluminescent substrate (Thermo Fisher-Pierce Protein Research Products, Rockford IL). (*Jason Hanna and Antonella Bacchiocchi grew Cell cultures. Matthew McRae did western blots with the guidance of Jason Hanna and Jennifer Bordeaux).*

Whole Section Analysis of Typical and Atypical Spitz Nevi, and Spitzoid Melanoma:

Dr. Rossitza Lasova and assistant Megan Keenan assembled a cohort of 20 typical Spitz nevi, 20 atypical Spitz nevi and 9 Spitzoid melanomas from the recently developed Yale Spitzoid neoplasm repository. This is the first repository of human Spitzoid neoplasm's in the world. Formalin fixed, paraffin embedded samples were cut, mounted on adhesive slides and dipped in paraffin for tissue preservation according to standard protocol. Slides were stored in nitrogen gas until staining. (*Spitz nevi, atypical Spitz nevi and Spitzoid melanoma cohort assembled and prepared for staining by Rossitza Lasova and Megan Keenan)*

Immunohistochemical Fluorescent Staining:

Slides were deparaffinized by incubation at 60°C. TMAs were "cooked" for 20 minutes while whole sections were incubated overnight. This was followed by two xylene exchanges. Slides were then rehydrated in sequential washes 100% ethanol, 100% ethanol, 70% ethanol and deuterium depleted water. The slides were transferred to 6.5mM Na-Citrate buffer (pH=6.0) and boiled in a pressure cooker for 10 minutes. An absolute methanol with 0.75% hydrogen peroxide solution for 30 minutes was used to quench endogenous peroxidase activity of the samples. After a wash in tap water, tris-buffered saline with tween (TBST) and finally tris-buffered saline (TBS), slides were incubated in 0.3% bovine serum albumin (BSA) in TBS for 1 hour at room temperature to diminish non-specific background staining. Two primary antibodies were used on

separate slides as the biomarker "target" of interest. Nedd 9/HEF1 mouse monoclonal IgG (Abcam, 18056, clone 2G9, Burlingame California) was diluted at 1:500 in BSA mixed with TBS. HMB45 mouse monoclonal IgG (Biogenex, AM001-5M, clone HMB45, San Ramon California) was manufactured pre-dilute.

The "tumor mask" was defined with rabbit polyclonal anti-S100B (DAKO Cytomation, Carpenteria, CA) at 1:200 to effectively delineate areas of tumor from surrounding tissue and stroma. For TMA slides stained with Nedd9 mouse monoclonal as a target only, HMB45 Rabbit monoclonal was added at 1:25 dilution to supplement S100 tumor mask. The solution containing BSA-TBST with "target" and "tumor mask" primary antibodies were aliquoted on each slide and incubated overnight at 4°C. Slides were then washed in two exchanges of TBS with Tween detergent and one wash of TBS. Envision goat anti-mouse horseradish peroxidase (Dako, Carpenteria California) was used as the secondary antibody to the target primary antibody (Nedd9 mouse, HMB45 mouse). Goat anti-rabbit conjugated Alexa 546nm (Molecular Probes, Eugene Oregon) was used a secondary antibody to the tumor mask primary antibody (S100 rabbit, S100 and HMB45 rabbit on TMA). Goat anti-rabbit Alexa 546 was diluted into the Envision mouse (neat) at a ratio of 1:100, aliquoted onto the slides and incubated for 1 hour, at room temperature. The fluorescent emission wavelength of the tumor mask was 570 nm.

Slides were then washed in TBST followed by TBS alone followed by incubation in cyanine-5-conjugated tyramide (Cy5) (Perkin-Elmer, Wellesley Massachusetts) for 10 minutes to activate the envision mouse horseradish peroxidase for amplified fluorescent visualization of the target primary antibody at 670nm (Nedd9 mouse monoclonal IgG antibody, HMB45 mouse monoclonal IgG antibody).

Slides were again washed in TBST followed by TBS and then incubated with 4', 6-diamidino-2-phenylindole (DAPI) at a dilution of 1:500 in 0.3%BSA-TBST for 20 minutes. Slides were then washed in TBST followed by TBS. Finally, slides were mounted with Prolong® Gold antifade reagent with DAPI (Invitrogen, Carlsbad California) and sealed with nylon-based lacquer. DAPI is a fluorescent stain that binds strongly to DNA with an emission maximum at 461nm. (*Matthew McRae did Immunohistochemical staining of TMAs and whole sections).*

Digital Image Capture and Automated Quantitative Analysis of Protein Expression (AQUA):

Stained slides were imaged on the HistoRX PM-2000™ (HistoRX, New Haven, Connecticut). This is a modified computer controlled epifluorescent microscope illuminated by a high-pressure mercury bulb (Photonic Solution, Mississauga Ontario) with a 4 megapixel thermoelectrically cooled monochrome CCD camera.

Image Grabber™ (HistoRX, New Haven, Connecticut) software was used for image acquisition of both TMAs and whole sections. The operator (Matthew McRae) first acquired a low-resolution image of the slide in the DAPI fluorescence channel. The region of sample on the slide was then selected. For TMA analysis, individual spots were located automatically with SpotGrabber™ (HistoRX, New Haven, Connecticut) followed by spot verification by the operator (Figure 2). For whole section analysis, the operator defined regions of interest manually, and the program then assigned a grid of high power fields (20X) for the entire specimen (Figure 3). The six images taken per tissue spot or

high-powered field are as follows: a DAPI channel showing the nucleus in the field of focus and 8 microns below the field of focus, a Cy3 channel showing the S100 tumor mask in the field of focus and several microns below the field of focus, a Cy5 channel showing either Nedd9 or HMB45 in the field of focus and 8 microns below the field of focus. A rapid exponential subtraction algorithm (RESA) subtracts the out of focus from the in-focus image to dramatically improve the assignment of pixels to a particular subcellular compartment (Figure 4).

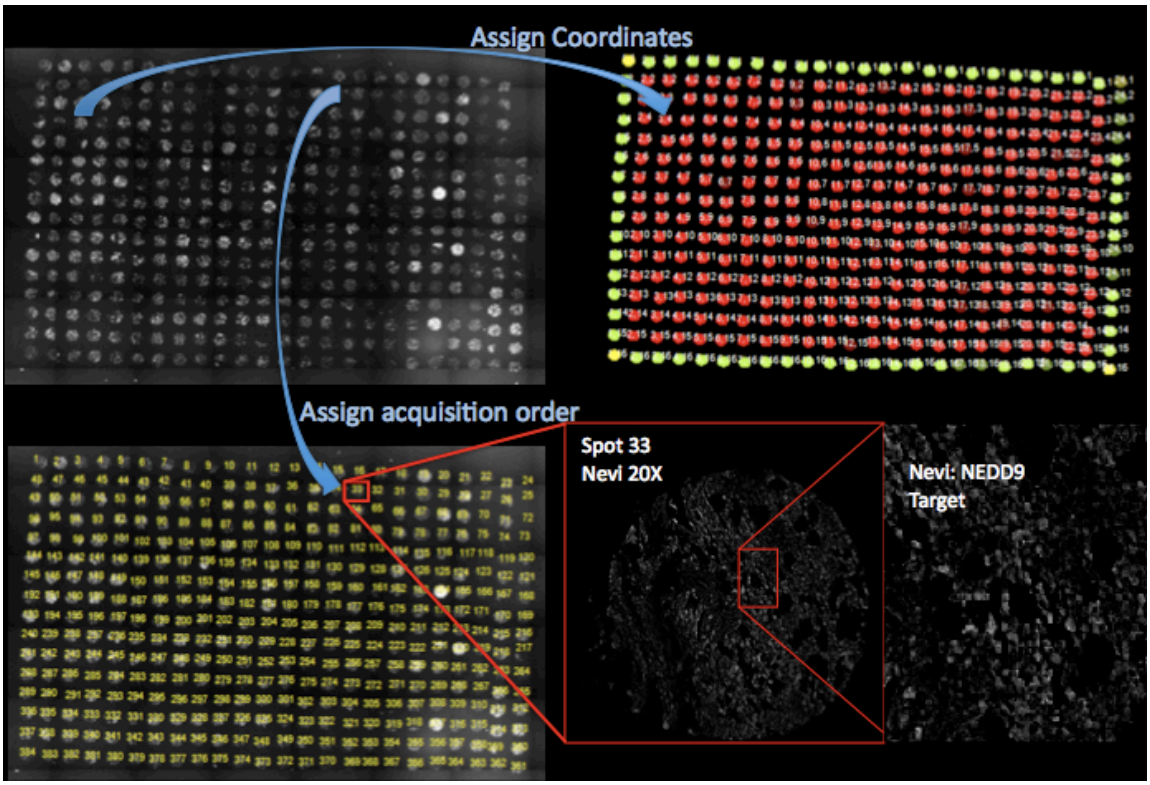

Figure 2: Low resolution DAPI image taken. SpotGrabber™ program then assigns both a grid number and an acquisition order for the HistoRX PM2000 microscope. At bottom right is a nevi at 20X from YTMA 66A stained with Nedd9 at 1:500 dilution and then further magnified to demonstrated staining pattern.

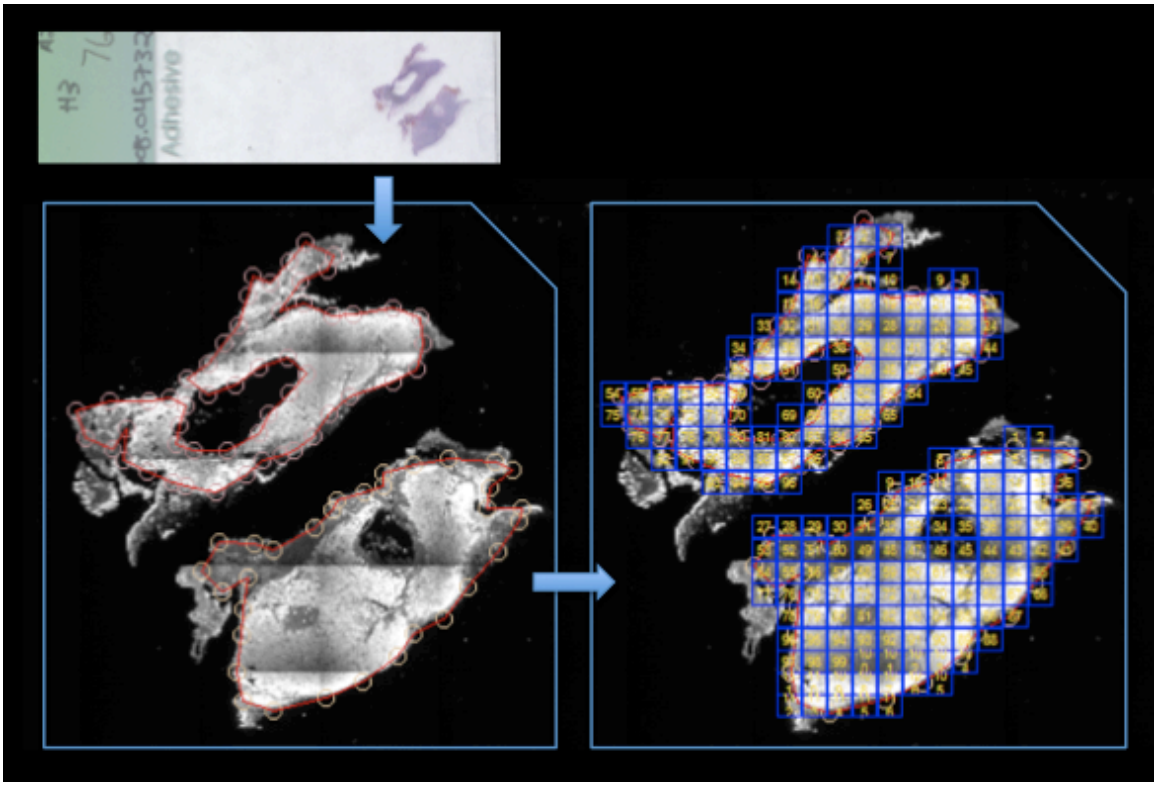

Figure 3: Low-resolution image of the whole section was taken, here of the S100 tumor mask. The operator assigns the region of interest by surrounding it with a series of dots connected by a red line. SpotGrabber™ then assigns a grid of high power fields that are acquired in assigned order.

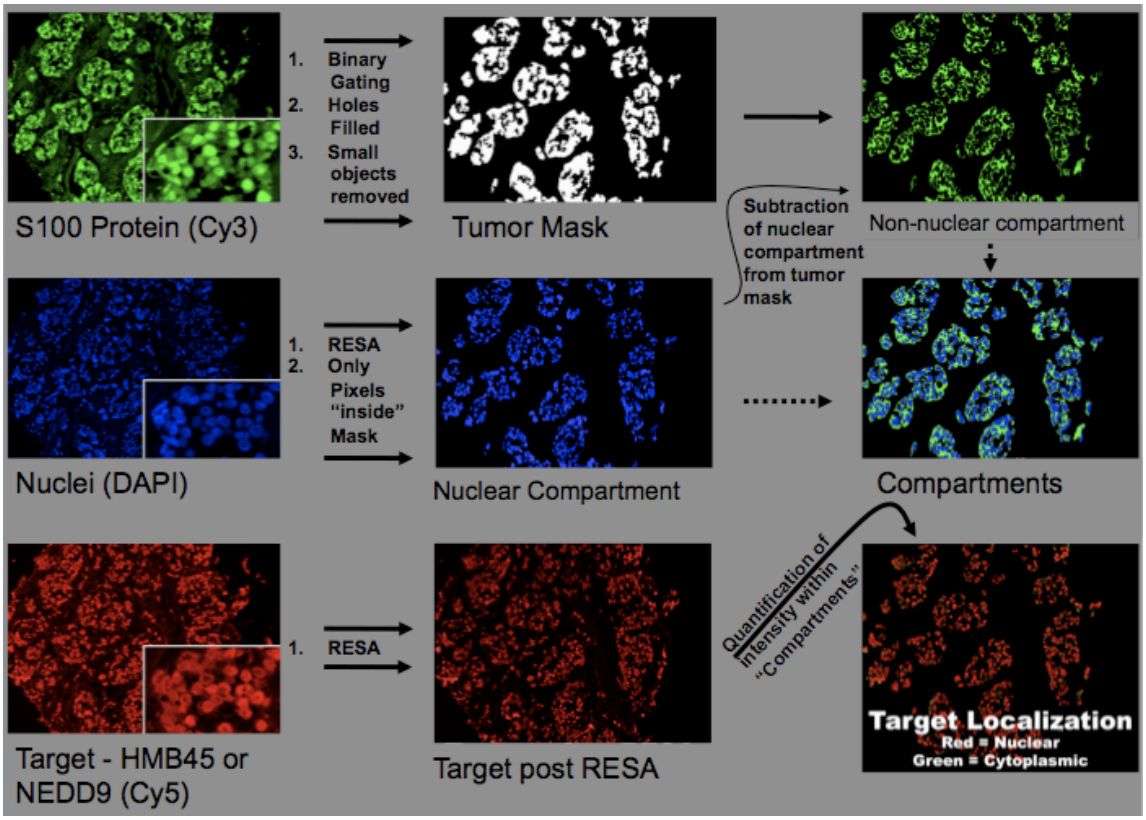

Figure 4: **S100 defines the tumor mask, DAPI defines the nuclear compartment and subtracting one from the other gives the non-nuclear compartment. The target of interest is read in the Cy5 channel. In this way compartments can be defined and an AQUA score generated as the intensity of target signal per pixel area of a region of interest. An AQUA score can be assigned to the tumor mask, the nuclear compartment or the non-nuclear compartment** (Adapted from Aaron Berger PhD committee meeting presentation[32]).

Exposure times were set for S100 tumor mask Cy3 channel at a level where roughly 25% of brightest spot on TMA or high power field in whole sections was saturated. The DAPI and Cy5 target of interest channel underwent auto-exposure controlled by the software program. The operator focused the microscope for the first spot (for TMA) or high power field (whole section) only as the microscope auto-focused on every spot and high-powered field according to the grid assigned prior to high power image acquisition.

Cellular compartments were formed by first defining the area of tumor from the surrounding stroma. Pixels were binary gated; meaning that a pixel is either positively

stained “tumor” or a negatively stained pixel is “not tumor”, in the Cy3, 570nm emission channel. Similarly the nuclear compartment (DAPI, 461nm emission) was binary gated as pixel that is positively stained and thus “nucleus” versus negatively stained “not nucleus.” Only nuclei within the tumor mask were measured. Finally the non-nuclear compartment was defined as the area within the tumor mask that was not nucleus.

After capturing the images, all TMA spots and high power fields of whole sections were reviewed to ensure proper staining. Certain spots and high power fields required cropping of the tumor mask and thus removal of that portion of the tumor for analysis. The reasons for a region to be cropped were as follows: non-specific staining of S100 mask such as with lymphocytes that were not in the tumor, folding of the sample on the slide resulting in out of focus imaging and altered AQUA scores, and discernable bubbles resulting from mounting and cover slipping.

With the subcellular compartments defined, quantitative analysis with AQUA® software (HistoRX, New Haven, CT) determined the level of fluorescence per pixel area on a scale from 0 to 33 000 according to tumor mask, nuclear compartment and non-nuclear compartment. An AQUA score is defined as the (intensity of target)/(area). The AQUA score was further normalized by exposure time and bit depth thus limited to signal emanating from the plane of focus. This represented a vast improvement of what pathologists commonly rely upon for analysis of IHC, which is generally a numeric score from 0 to 4 varying with level of expression subjectively judged by the naked eye. (*Matthew McRae completed AQUA analysis with the help of Jason Hanna, Elsa Anagnostou, and Eirini Pectasides).*

Statistical Analysis

TMA spots and whole section high power fields whose mask covered less than 5% of the total field area were removed from the analysis. Spots and high power fields without adequate compartmentalization as determined by a ratio of nuclear to non-nuclear DAPI of under 1.5 were also discarded. Exclusion was necessary because despite UV cross-linking to the slide, the 0.6 mm histospots sometimes fell off the slide or were badly folded or damaged during staining. The reason for poor compartmentalization was that the AQUA algorithm was optimized for capture of the entire array and was not adjusted for each individual spot. As a result, there were spots that fell outside of the optimized range for compartmentalization.

Pearson's correlation coefficient (R) was used to assess the correlation between AQUA scores from the same cores on serial cuts of the control array; an R^2 greater than 0.8 was indicative of excellent intra-array reproducibility.

For TMA analysis, each tissue spot received an AQUA score according to subcellular compartment and tumor mask. To compare the intensity of nuclear to non-nuclear staining, the natural log of the ratio of nuclear to non-nuclear AQUA scores was calculated. This was defined as the "subcellular AQUA ratio." For whole section analysis, a median, mean, maximal and minimal score was taken for each tumor sample. The median score was used to compare the natural log of the ratio of nuclear to non-nuclear AQUA scores.

The ratio of nuclear to non-nuclear staining across the progression of melanocytic

lesions was performed by the analysis of variance (ANOVA). Testing for the significance of individual pair wise comparisons of each ANOVA was adjusted using the Tukey post hoc method for multiple comparisons. Calculation of the receiver-operator characteristic curve (ROC) for Spitz neoplasms was performed from the logistic regression model measuring the likelihood that a given sample is a benign Spitz Nevus. For all analyses, significant associations were defined as $p<0.05$. All statistical analysis was performed using Statview 5.0.1 (SAS Institute Inc., Cary, NC) and SPSS software program (version 13.0 for Windows, SPSS Inc., Chicago, IL). (*Statistical analysis done by Matthew McRae and Elsa Anagnostou)*

Ethical Use of Human Subjects

This research protocol involved the use of tissue taken from human subjects as well as clinical data related to their diagnosis. This protocol was approved by the Yale Human Investigations Committee for the assessment of predictive and prognostic biomarkers in cancer (HIC Protocol #9505008219).

Results

Antibody Validation

NEDD9

Titering on YTMA 109 test array and YTMA 112 resulted in an ideal concentration determined for specific staining of NEDD9 antibody at 1:500. This is consistent with previous validation done in the Rimm laboratory by William Bradley (unpublished results).

These results were validated on YTMA 98-2 Boutique Array. The boutique array contains the MCF-7 cell line. Despite being a breast cancer cell line, it specifically expressed cytoplasmic Nedd9 *in situ.* In addition, all of the melanoma cell lines showed specific cytoplasmic staining. A western blot was used to verify the expression of Nedd9 in the MCF7 cell line as well as in the melanoma cell line Mel888 cell lines (Figure 5).

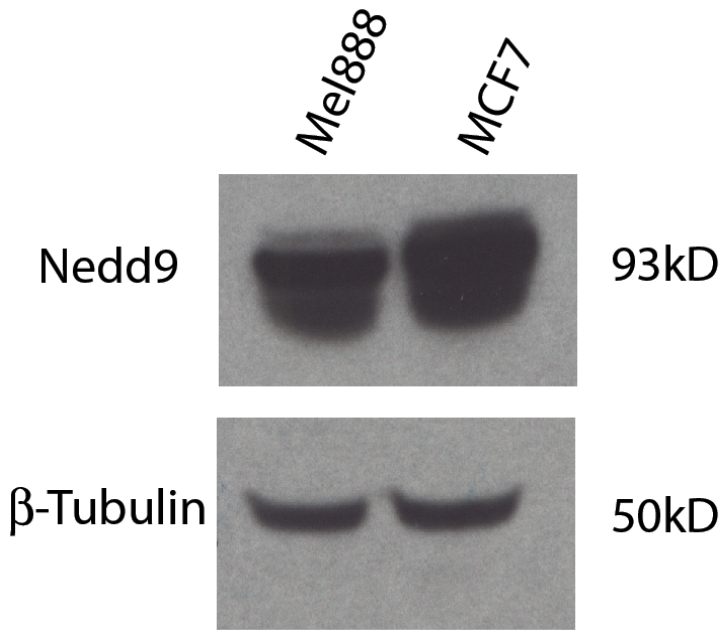

Figure 5: Western blot of Mel888, a melanoma cell line and MCF7, a breast cell line. Both cell lines express Nedd9 protein. Nedd9 is 93kD.

Nedd9 expression in benign nevi showed specific staining with lower level AQUA scoring in the tumor mask compared to primary melanoma and showed a propensity to the nuclear compartment of the cell. As a proxy for benign nevi, a lysate was prepared of cultured human foreskin melanocytes and the Western blot verified detectable level of Nedd9 expression (Figure 6).

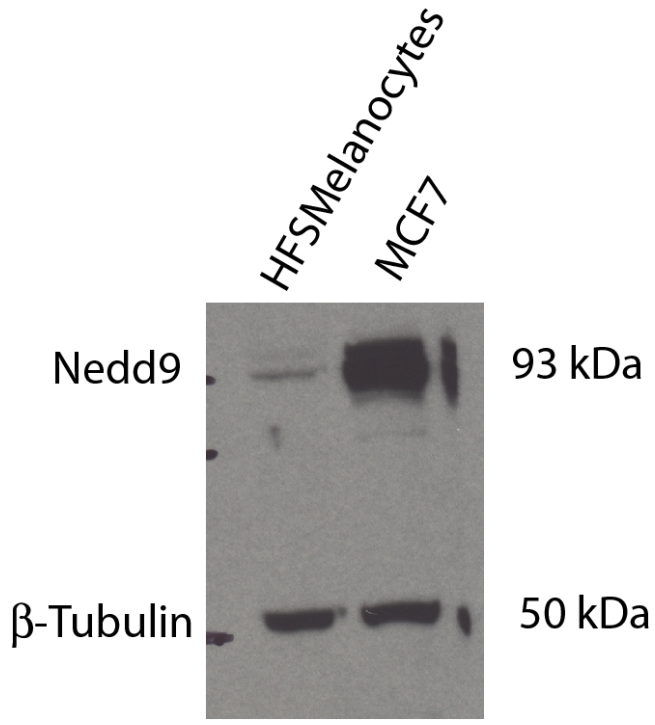

Figure 6: Western blot of MCF7 cell line lysate and lysate from human foreskin melanocytes. Primary Antibody NEDD9 at 1:2000. Nedd9 is a 93 kDa protein.

HMB45

The HMB45 antibody had already undergone extensive validation in our laboratory [20] however titering of HMB45 on test arrays verified the ideal dilution to be the pre-dilute stock solution. It was then stained on YTMA 98-2 cut 60 for validation on cell lines prior to experiments using whole sections.

The Subcellular AQUA Ratio for Diagnosing Benign versus Malignant Tumor Type

NEDD9: YTMA 98-2

Beyond the utility of this array for antibody validation and to assess for both inter and intra-array reproducibility and specificity of antibody staining, the Yale boutique array had a variety of tumor specimens including benign nevi, primary melanoma and metastatic melanoma. The distribution of the subcellular AQUA ratio of benign nevi and primary melanoma is shown in Figure 7. Unpaired t-test was used to compare the benign nevi versus primary melanoma (Figure 8). We demonstrated a clear difference between the average subcellular AQUA ratio[1] of Nedd9 between benign nevi (mean=-0.429, std dev=0.108) and primary melanoma (mean=-0.645, std dev=0.293).

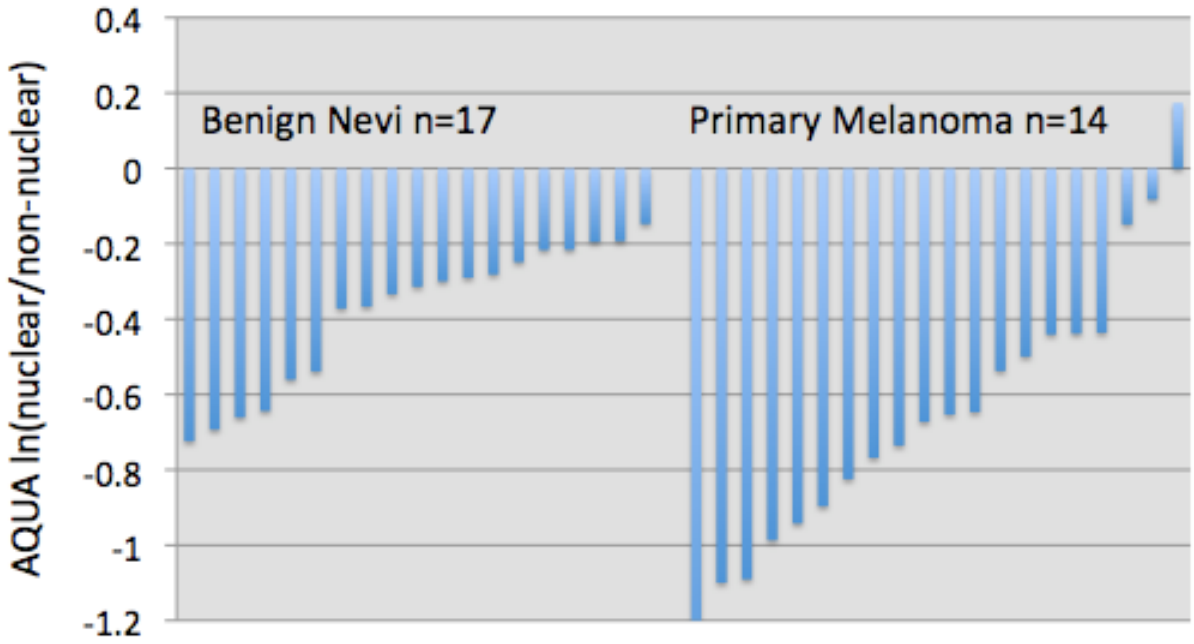

Figure 7: Distribution of median subcellular AQUA ratio for NEDD9 on YTMA 98-2 Cut 53. The two tumor types analyzed were benign nevi and primary melanoma.

[1] Subcellular AQUA ratio = the natural log of the AQUA score in the nuclear compartment of the cell divided by AQUA score in the non-nuclear compartment of the cell.

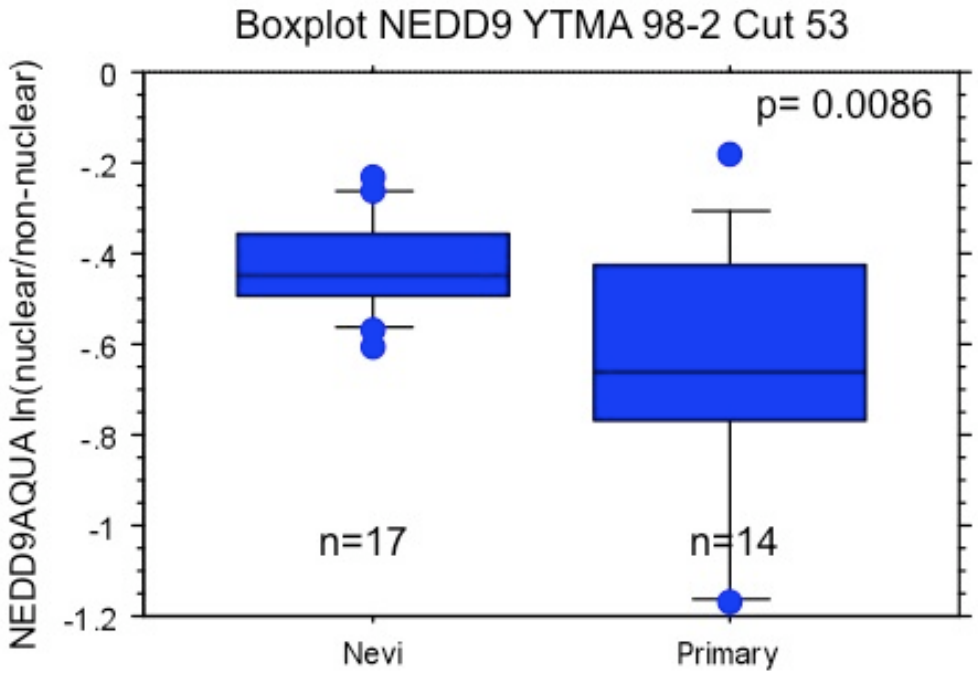

Figure 8: Boxplot from TMA 98-2 of the subcellular AQUA ratio of nevi versus primary melanoma stained with NEDD9 at 1:500. [2]

NEDD9: YTMA 66A

Regression analysis between cell lines of preparatory YTMA 98-2 boutique cut 46 and positive control serial section YTMA 98-2 boutique cut 47 stained with YTMA 66A showed excellent reproducibility with a Pearson correlation coefficient squared (R^2) between validation and experiment of 0.8241.

This array was used to verify the staining pattern across a wide variety of benign nevi and to directly compare these to metastatic melanoma controls. Figure 9

[2] The box of the boxplot itself represents the inter-quartile range (from the 25th to 75th percentile) of AQUA scores for all the tumor spots of a specified tumor type. The line in the middle of the box is the median score. The t-bars extend to the furthest score that is within 1.5 times the inter-quartile range from both ends of the box. Beyond the t-bars, scores are considered outliers.

demonstrates the staining of Nedd9 in a nevus (a) versus a metastatic melanoma (b). Note the heavily cytoplasmic and membranous stain of Nedd9 in the metastatic melanoma versus the more nuclear stain of the Nevi.

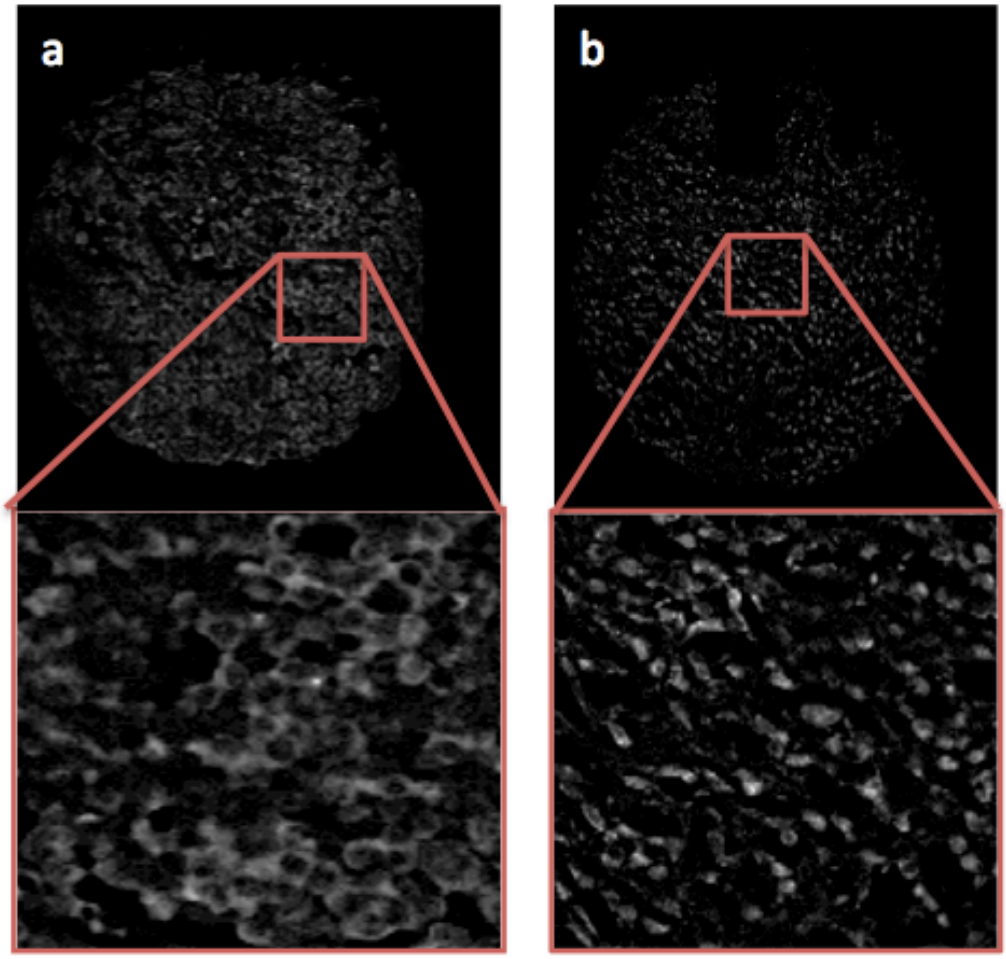

Figure 9a: Melanoma Metastasis, Nedd9 target **Figure 9b: Benign Nevi, Nedd9 target**

The distribution of the subcellular AQUA ratio of benign nevi and primary melanoma is shown in Figure 10. Figure 11 is a box plot demonstrating the differential expression of Nedd9 in the nuclear to non-nuclear compartment of the cell according to tumor type. Of the 299 nevi, 79 were excluded from analysis due to inadequate sample or

inadequate subcellular compartmentalization of the cell as assessed by DAPI staining within the cytoplasmic compartment. Of the 40 metastatic melanoma samples, 3 were excluded.

We found that the mean value of the subcellular AQUA ratio was higher for nevi (mean=-0.342, std dev=0.159) when compared to the melanoma metastases (mean=-0.482, std dev=0.149). Unpaired t-test analysis demonstrated a p value of <0.0001. The subcellular AQUA ratio for Nedd9 can differentiate benign nevi from metastatic melanoma (Figure 11).

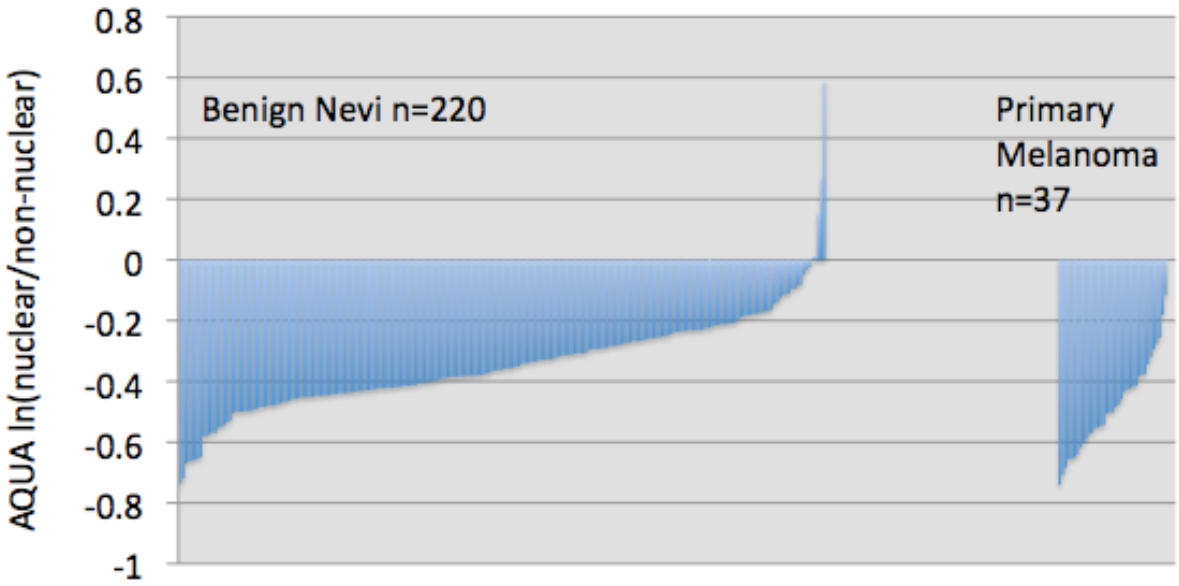

Figure 10: Distribution of median subcellular AQUA ratio for NEDD9 on YTMA 66A. The two tumor types analyzed were benign nevi and melanoma metastases.

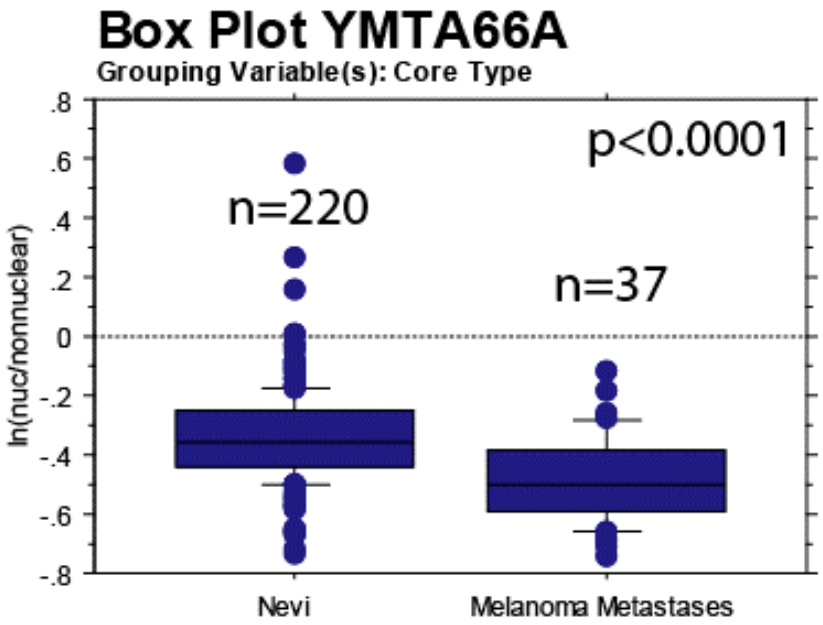

Figure 11: Boxplot showing the subcellular AQUA ratio of benign nevi versus melanoma metastases from YTMA 66A nevi array stained with NEDD9 at 1:500.

NEDD9: SPORE 84 Array

Regression analysis between cell lines of preparatory YTMA 98-2 boutique cut 44 and positive control serial section YTMA 98-2 boutique cut 45 stained with SPORE 84 showed excellent reproducibility with an $R^2 = 0.8622$ between validation and experiment. 54 of 87 benign nevi, 112 of 136 primary melanoma and 128 of 146 melanoma metastases originally on the TMA were suitable for scoring (Figure 12).

The SPORE array was stained with Nedd9 1:500 with differential AQUA scores according to tumor type. The distribution of the subcellular AQUA ratio of benign nevi, primary melanoma and melanoma metastases are shown in Figure 13. Benign nevi had a count of 54 samples with a mean subcellular AQUA ratio of -0.319 (std. dev.= 0.141). Primary melanomas had a final count of 112 with a mean score of -0.435 (std.

dev.=0.185) Metastatic melanoma had a final count of 128 with a mean score of -0.42 (std. dev.=0.188). There was a significant difference between tumor types by ANOVA with a p-value of 0.0003 (Figure 14).

Fisher's PLSD showed a p-value of 0.0001 between nevi and primary melanoma with a p-value of 0.0006 for nevi and melanoma metastases. Tukey/Kramer post hoc analysis showed a significant difference between nevi and primary melanoma and between benign nevi and melanoma metastasis with significance set at 5%. There was no measurable difference between primary melanomas and melanoma metastases. This shows in a large independent cohort that the subcellular AQUA ratio is useful in differentiating benign nevi from malignant primary and metastatic melanoma lesions.

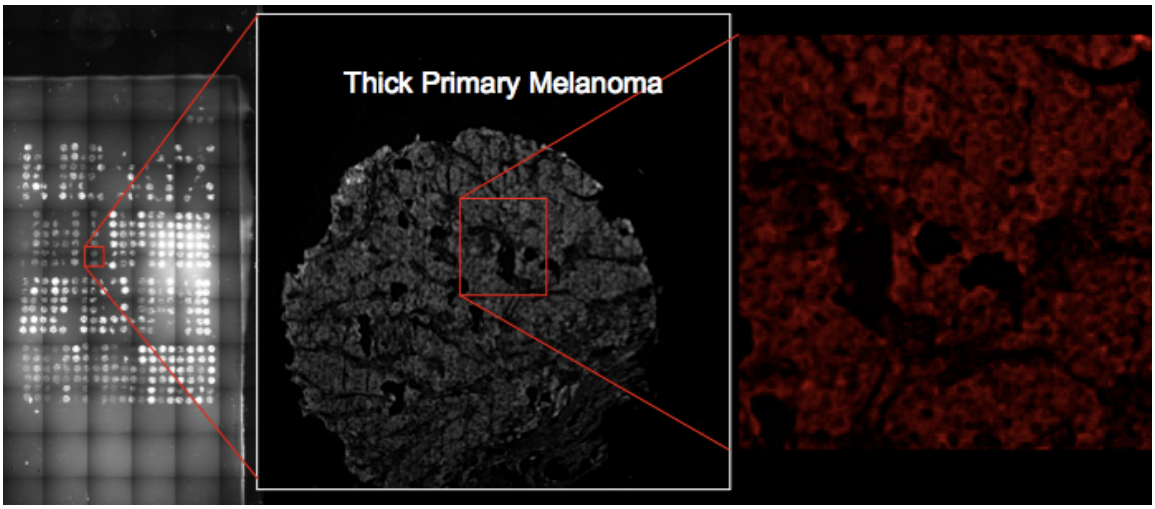

Figure 12: At left is the entire array captured at low resolution on the DAPI fluorescence channel. Magnified at 20X is a core from the SPORE 84 array that represents a thick primary melanoma. This is further magnified to demonstrate the non-nuclear staining characteristic of primary melanoma tumor cores on this array.

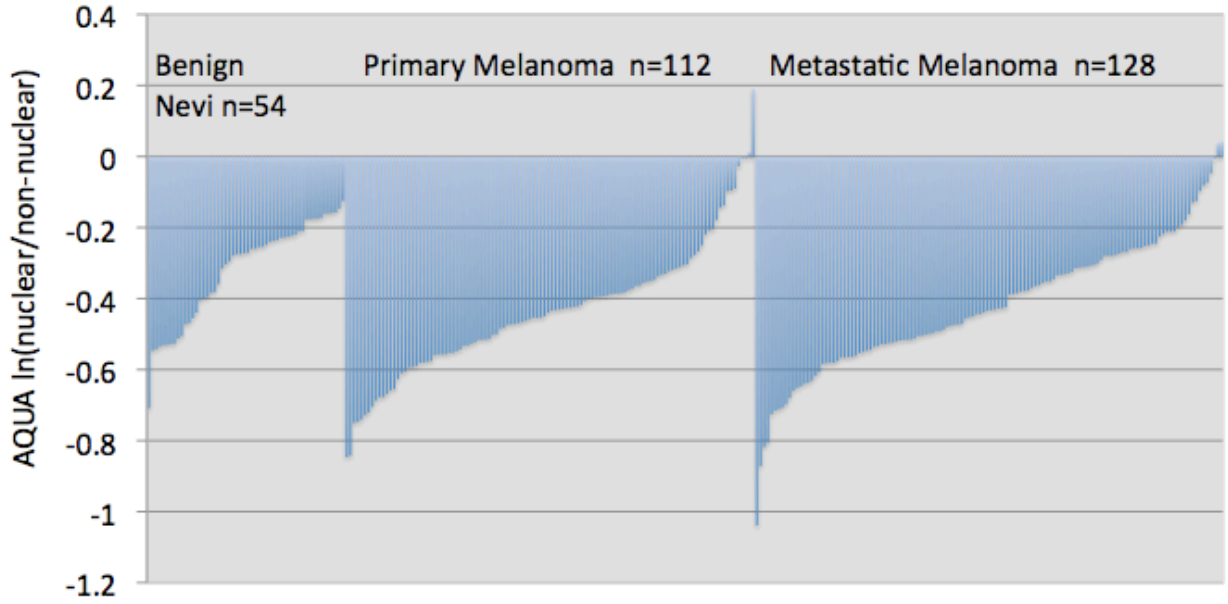

Figure 13: Distribution of median subcellular AQUA ratio for NEDD9 on SPORE 84 array. The three tumor types analyzed were benign nevi, primary melanoma and melanoma metastases.

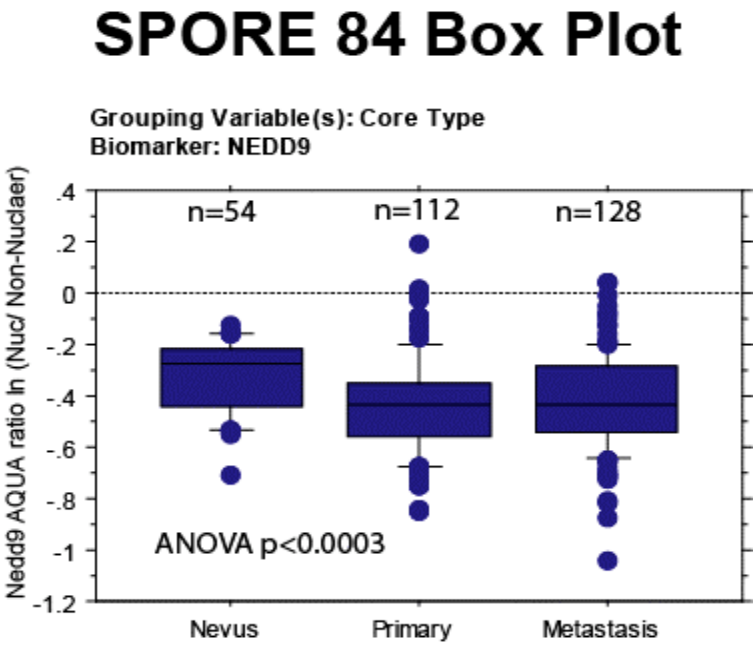

Figure 14: Boxplot of NEDD9 staining at 1:500 dilution on SPORE 84 array. The subcellular AQUA ratio is significantly less in malignant primary and metastatic melanoma versus benign nevi.

HMB45: YTMA 98-2

After titering and validation on test arrays, YTMA 98-2 cut 60 was stained with HMB45 predilute primary antibody to verify staining on cell lines and on surgical specimens of primary melanoma that could serve as a control for the whole section Spitz nevi experiment.

The distribution of the subcellular AQUA ratio of benign nevi and primary melanoma is shown in Figure 15. The progression from benign nevi (mean=-0.159, std. dev.=0.158) to primary melanoma (mean=-0.463, std. dev.=0.264) showed a significant difference in the subcellular AQUA ratio. This was significant by unpaired t-test at a p=0.0001 (Figure 16).

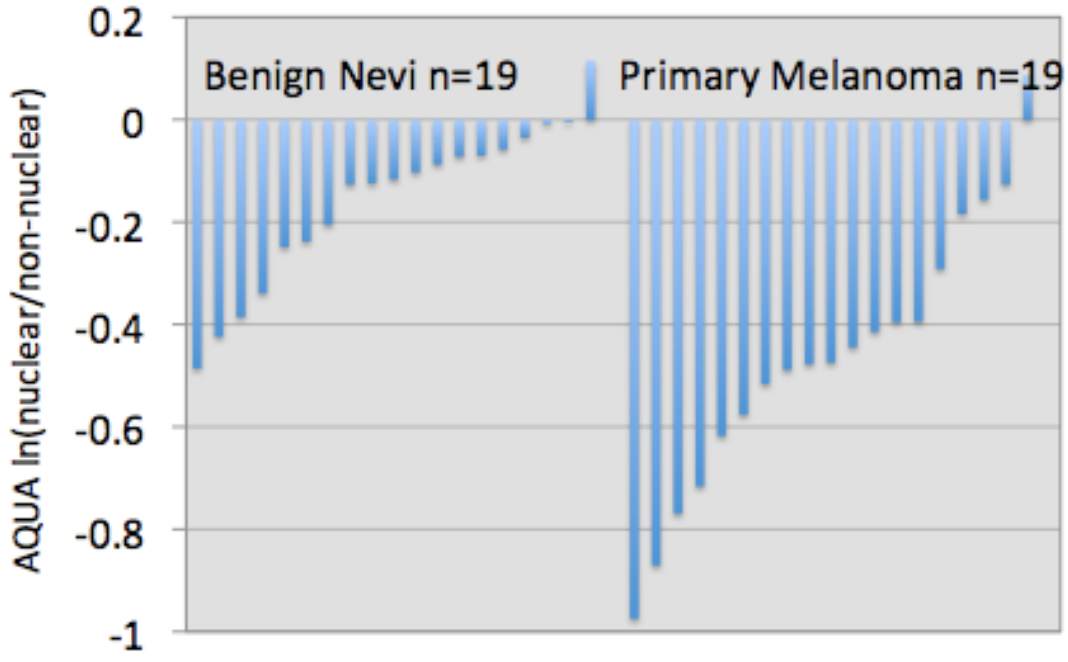

Figure 15: Distribution of median subcellular AQUA ratio for HMB45 on YTMA 98-2 Cut 60. The two tumor types analyzed were benign nevi and primary melanoma.

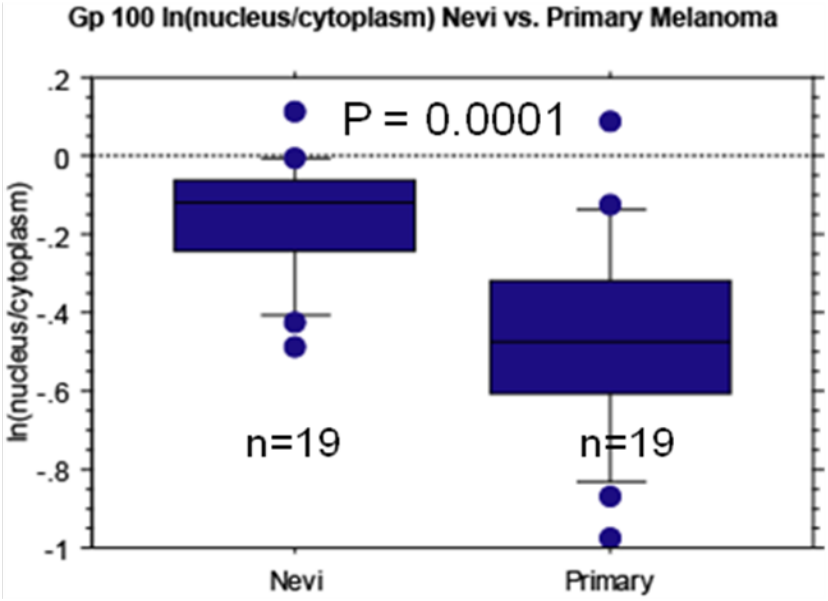

Figure 16: Boxplot of the subcellular AQUA ratio from YTMA 98-2 of nevi versus primary melanoma stained with HMB45.

Testing Subcellular AQUA Ratio for Benign vs. Malignant on Spitz Nevi, Atypical Spitz Nevi and Spitzoid melanoma

Nedd9 Whole Section Analysis

Regression analysis between cell lines and surgical specimens of preparatory YTMA 98-2 boutique cut 52 and positive control serial section YTMA 98-2 boutique cut 53 stained with whole sections that included whole section analysis of 20 Spitz Nevi, 20 atypical Spitz Nevi and 9 Spitzoid melanoma, showed good reproducibility of antibody staining with a Pearson correlation squared (R^2) between validation and experiment at 0.5802.

The distribution of the median subcellular AQUA ratio of all high power fields (20X) per whole section according to tumor type is shown in Figure 17. There is no statistically significant difference between the distributions of the scores according to tumor type. The mean subcellular AQUA ratio for tumor types were as follows: Spitz nevi=-0.169 (std. dev.=0.213), atypical Spitz nevi=-0.036 (std. dev.0.278), Spitzoid Melanoma=-0.012 (std. dev.=0.323) (Figure 18). NEDD9 staining of a benign Spitz nevi and a Spitzoid melanoma are demonstrated in Figure 19.

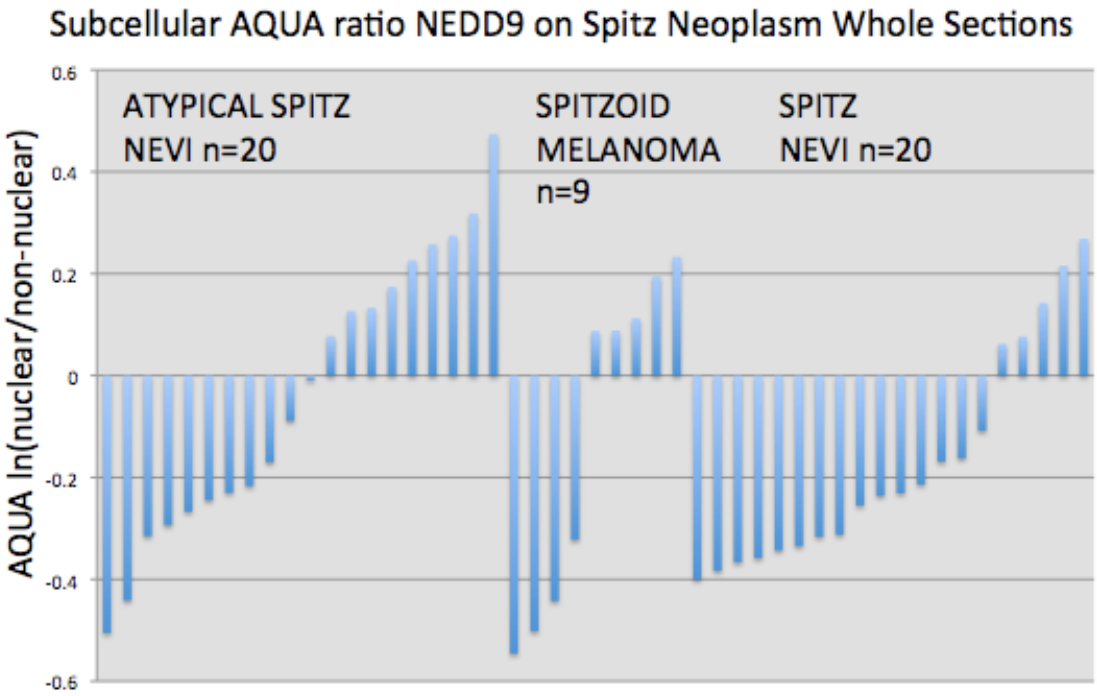

Figure 17: Distribution of median subcellular AQUA ratio for NEDD9, 1:500 dilution. The three tumor types analyzed were atypical Spitz, Spitzoid melanoma and typical Spitz nevi.

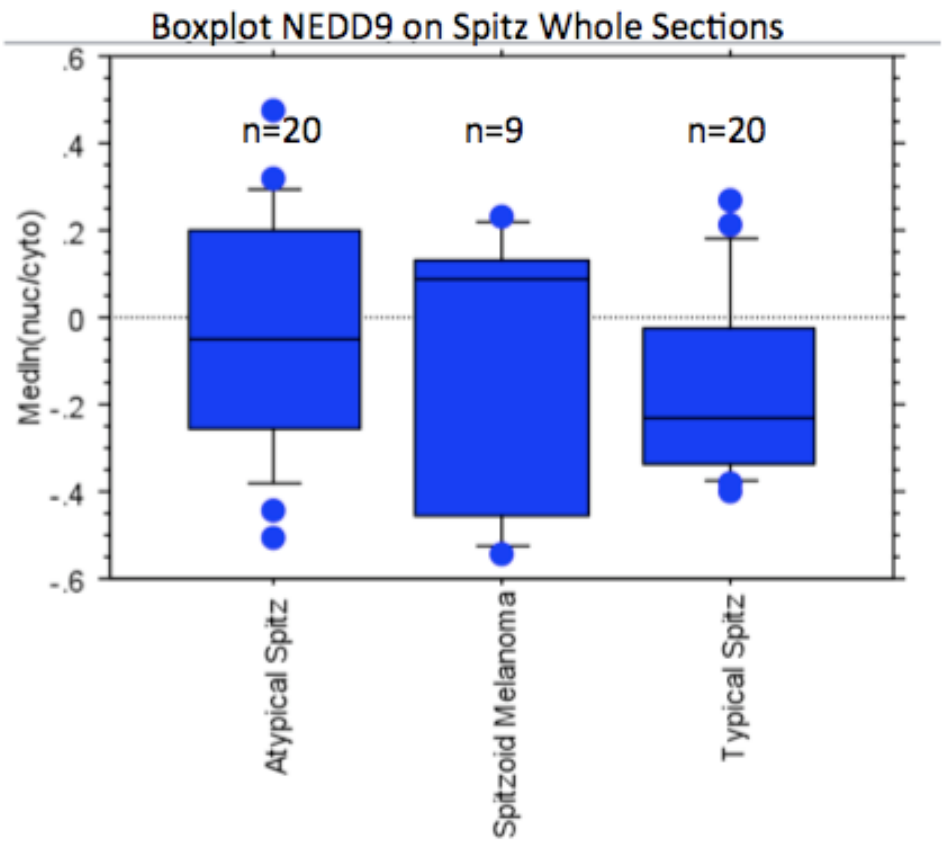

Figure 18: Boxplot of Median value of Nedd9subcellular AQUA ratio. No significant difference was detected by tumor type with Turkey/Kramer post-hoc not attaining statistical significance with p>0.05.

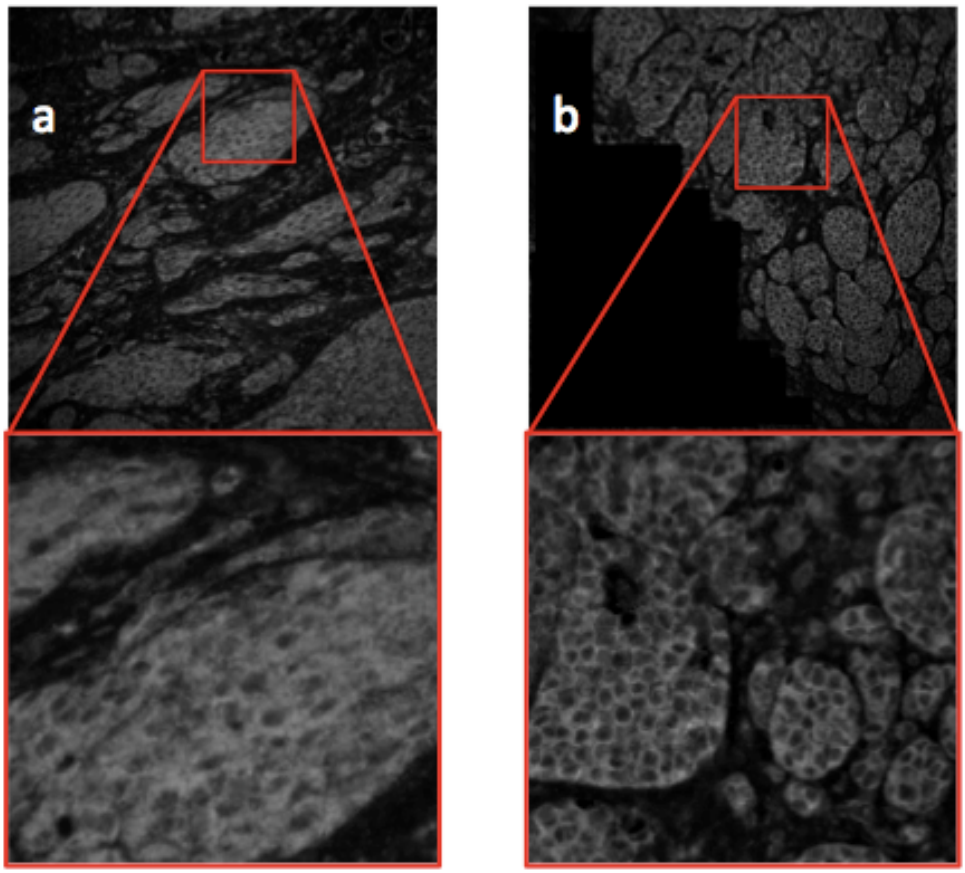

Figure 19 a is an example of a single high-powered (20X) field of a benign typical Spitz nevi stained with NEDD9 and a small region further magnified to appreciate the staining pattern. Figure 19b is an example of a single high-powered (20X) field of a malignant Spitzoid melanoma with a small portion further magnified.

HMB45 Whole Section Analysis

Regression analysis between cell lines and surgical specimens of preparatory YTMA 98-2 boutique cut 60 and positive control serial section YTMA 98-2 boutique cut 61 stained with whole sections that included 20 Spitz nevi, 20 atypical Spitz nevi and 9 Spitzoid melanoma, showed excellent reproducibility of antibody staining with a Pearson correlation squared (R^2) between validation and experiment at 0.8486.

The distribution of the median subcellular AQUA ratio of all high power fields (20X) per whole section according to tumor type is shown in Figure 20. There is no statistically significant difference between the distributions of the scores according to tumor type. The mean subcellular AQUA ratio for tumor types were as follows: Spitz nevi= -0.502 (std. dev. 0.316), atypical Spitz nevi= -0.31 (std. dev.=0.26), Spitzoid melanoma=-0.535 (std. dev.=0.32) (Figure 21). HMB45 staining of a benign Spitz nevi and a Spitzoid melanoma are demonstrated in Figure 22.

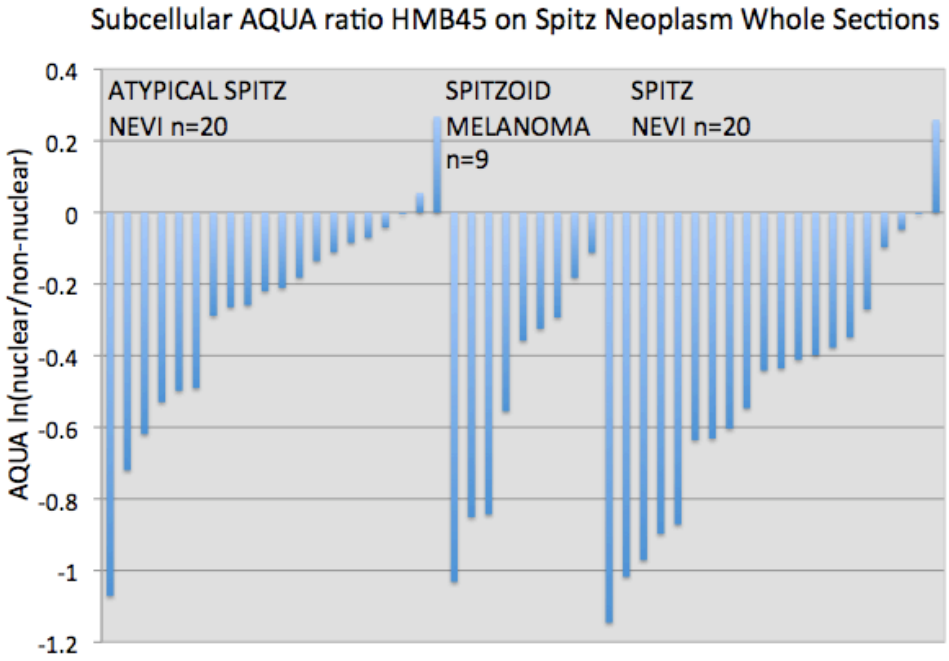

Figure 20: Distribution of subcellular AQUA ratio for HMB45. The three tumor types analyzed were atypical Spitz, Spitzoid melanoma and typical Spitz nevi.

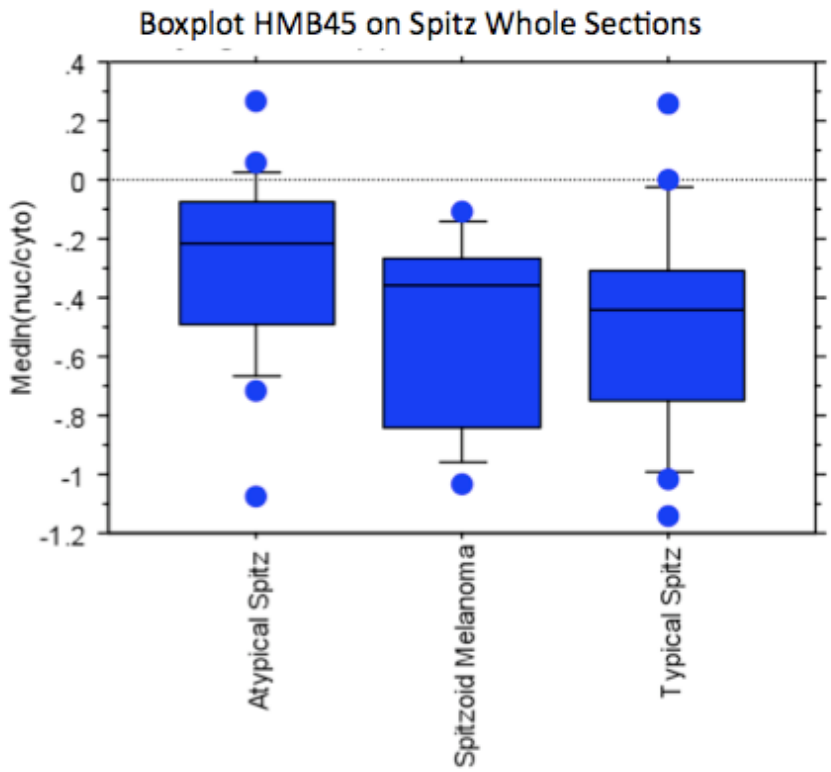

Figure 21: Boxplot of Median value of HMB45 subcellular AQUA ratio. No significant difference was detected by tumor type. Turkey/Kramer post hoc analysis was not significant with p>0.05.

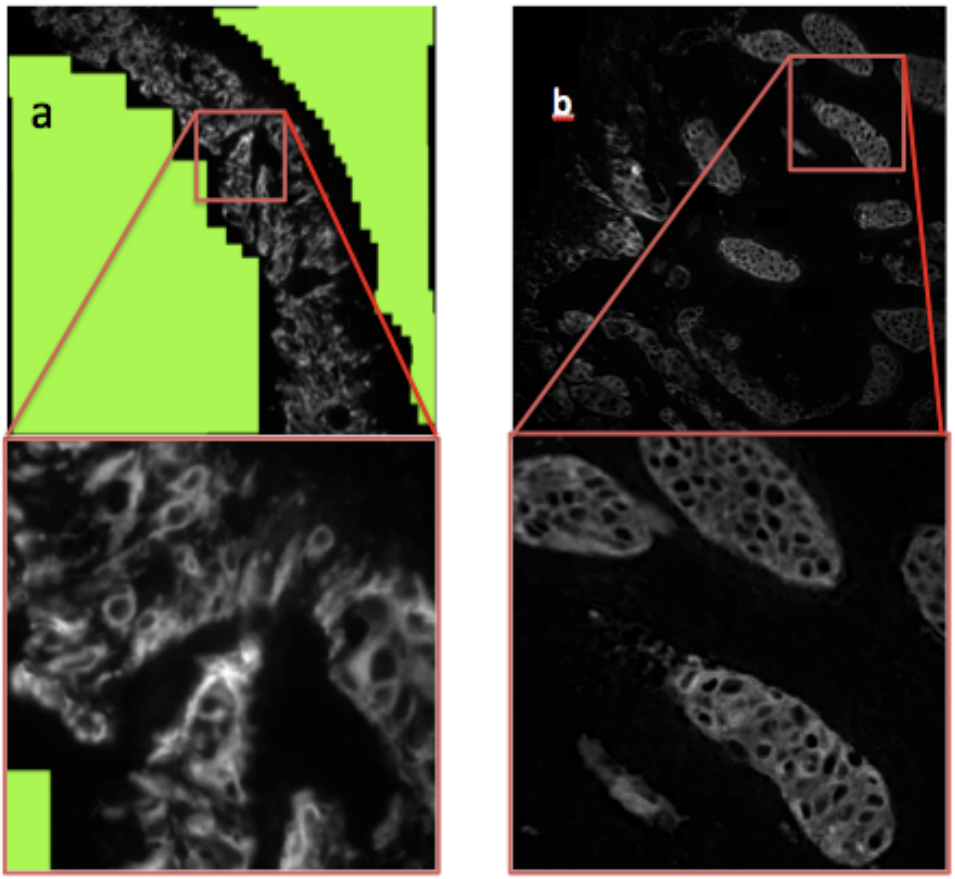

Figure 22: (a) is an example of a single high-powered (20X) field of a benign atypical Spitz nevi stained with HMB45 and a small region further magnified to appreciate the staining pattern. (b) Is an example of a single high-powered (20X) field of a malignant Spitzoid melanoma with a small portion further magnified

Discovery Analysis: HMB45 Maximum

The maximum HMB45 AQUA score in the tumor mask (figure 23) for a single high power field was able to differentiate between Spitzoid melanoma and both atypical and typical Spitz nevi.

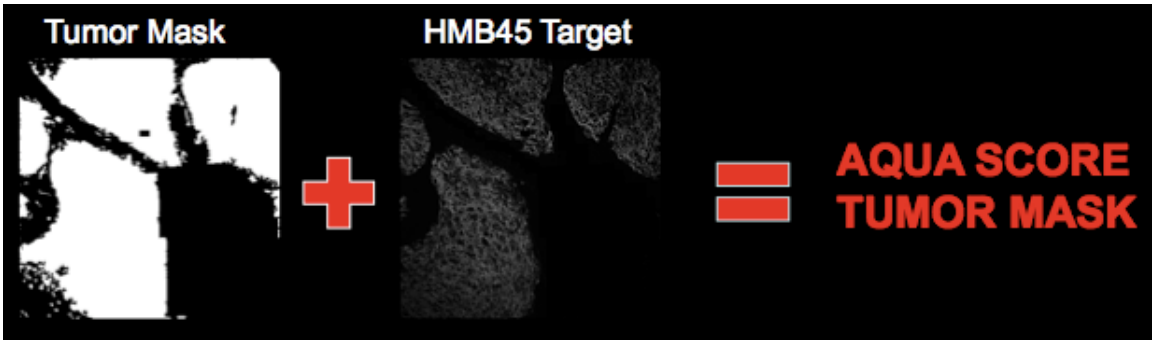

Figure 23: The tumor mask on the left defines the area of tumor. The HMB45 Target is then measured only if the pixels co-localize where tumor is present. The maximum total score of a single high-powered field was looked at using discovery analysis for the entire cohort.

Nine Spitzoid melanomas had a mean maximum AQUA score of 825.7 (standard deviation 686.6) while the 40 benign Spitz tumors had a mean maximum AQUA score of 418.554 (standard deviation 304.5). Unpaired t-test resulted in a p value of 0.0077 (Figure 24).

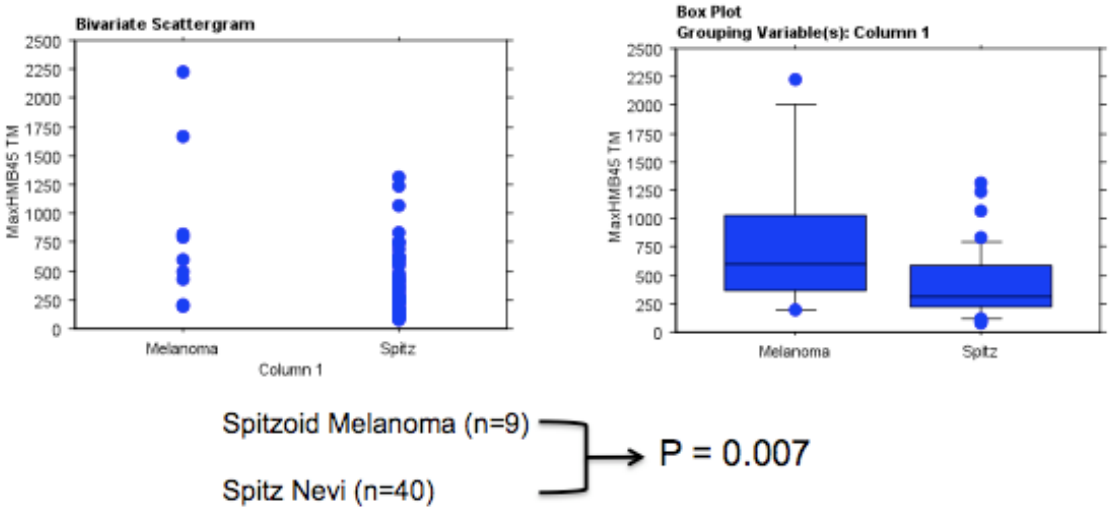

Figure 24: Bivariate scatter gram shows the distribution of maximum AQUA score per whole section tissue sample for benign Spitz nevi (both atypical and typical) and melanoma with Spitzoid features. Box plot shows the same data with box and T-bar.

Logistic regression of maximum score of a high power field in a tumor sample permitted the construction of a receiver operating characteristic curve. Area under the curve can be interpreted as the probability that when we randomly pick Spitzoid melanoma and a benign Spitz tumor, the classifier will assign a higher score to the Spitzoid melanoma than to the benign Spitz tumor (Figure 25).

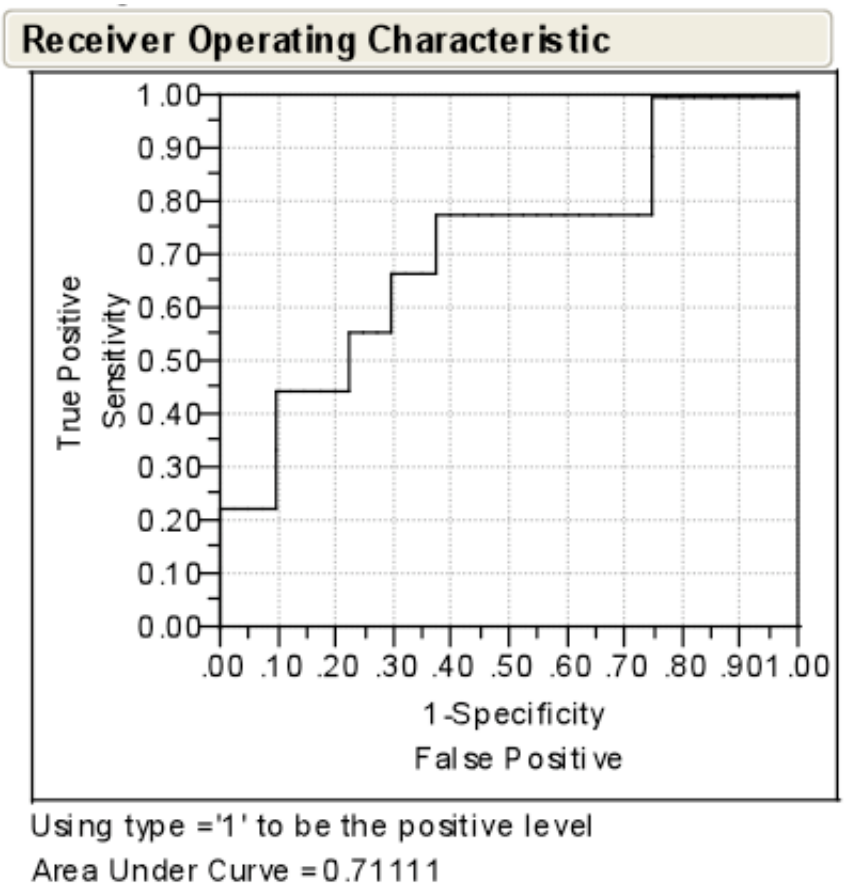

Figure 25: Receiver Operating Characteristic curve with true positive versus false positive. The area under the curve=0.711.

Discussion

Nedd9 and HMB45: Benign nevi, Primary and Metastatic Melanoma on Tissue Microarray

Published reports on Nedd9 suggested a role for this protein in melanoma metastasis as well showing an increase in tumor expression as tumors progress from benign to primary and to metastatic melanoma by IHC[25]. However, the method of IHC was limited to semi-quantitative, subjective, chromogen stained slides. We did a similar analysis but instead used fluorescence IHC technique that permitted the automated, quantified, reproducible reading of expression levels that can be quantified on a continuous scale. The analysis of expression level of Nedd9 was more carefully quantified by the AQUA score within the entire tumor (tumor mask) and the two subcellular compartments. The adoption of this technology all but eliminates interpretation bias.

NEDD9 staining on YTMA66A confirmed the published literature of high levels of Nedd9 expression in melanoma metastases. By forming a nuclear compartment, the "patchy" staining of benign nevi reported was localized predominantly to the nuclear or at least peri-nuclear region. This low level expression would likely not be appreciated by traditional chromogen staining with hematoxylin counter stain.

The subcellular localization in our analysis was not perfect. While to the eye, expression appeared predominantly nuclear, the absolute levels of Nedd9 expression generally favored the non-nuclear compartment even in benign nevi.

Despite a small cohort size, YTMA 98-2 allowed for a comparison of Nedd9 expression between benign nevi and primary melanoma. This quantified and substantiated the claim of differential expression by tumor progression and suggested that NEDD9 is not only a marker of melanoma metastasis but of progression from a benign to a malignant state. The SPORE 84 array was a large independent cohort on which the hypothesis of differential expression of subcellular compartments, measured by the subcellular AQUA ratio, was powered to view relevant variance in expression by tumor type. There was a similar ratio of expression levels in the subcellular compartments in both primary and metastatic melanoma. The ratio of expression was significantly different however between benign nevi and primary melanoma and between benign nevi and metastatic melanoma. The subcellular AQUA ratio score for Nedd9 was valuable for distinguishing benign versus malignant, however it was not able to distinguish melanoma progression from primary to metastatic.

Rothberg defined the differential staining pattern by subcellular compartment through forming a ratio of the nuclear to non-nuclear compartments and normalizing these scores by their natural log. We describe this ratio in this report as the subcellular AQUA ratio. HMB45 has been shown conclusively to have the ability to discern between benign and malignant by the subcellular localization of IHC using fluorescence [20]. In validating their data, we noted that while the values between tissue core types remained statistically significant, the y-axis was shifted for the benign nevi to a median subcellular AQUA ratio of below zero. This observation can be accounted for in two ways. One is that the subcellular localization in AQUA 1.6® software (HistoRX, New Haven, CT) can only be optimized for an entire array encompassing many tumor spots. Previous versions

of the software, including that done by Rothberg *et al* permitted optimization for every spot. This could account for a more tailored compartmentalization and less leakage of nuclear stain being interpreted as "non-nuclear." This is an inherent difficulty in optimizing an automated system. High throughput, reproducible measurements replace subjective interpretation of compartmentalization assigned by a technician. The second possible explanation for the score shift is that we employed a new AQUA technology that uses an algorithm to standardize the AQUA score by exposure time. This was a change from the prior experiment as Image Grabber™ (HistoRX, New Haven, Connecticut) used auto-exposure time to optimize exposure times for each histo-spot that was not possible with prior editions of the software. While both of these explanations account for the variation in AQUA scores between our experiment and that of Rothberg *et al.* for HMB45, it is ultimately not of clinical importance as the difference between benign nevi and both primary and metastatic melanoma are maintained.

NEDD9 and HMB45 reliably differentiated benign nevi from malignant melanoma on tissue microarray analysis using the subcellular AQUA ratio.

Whole Section Analysis: Spitz Nevi, Atypical Spitz Nevi, Spitzoid Melanoma

Both NEDD9 and HMB45 were chosen for whole section analysis of Spitz lesion due to their potential role in melanoma progression. Initial studies completed with both biomarkers in our laboratory demonstrated a similar pattern of staining. The benign nevi on tissue microarray had nuclear staining while primary and metastatic melanoma had a cytoplasmic and membranous staining pattern. The subcellular AQUA ratio of tissue

samples were compared and demonstrated that NEDD9 subcellular AQUA ratio had a comparable ability as HMB45 to differentiate benign nevi from melanoma.

Before moving to full section analysis of Spitz tumors, it was first necessary to prove differential expression of biomarker expression, in unambiguous terms, between benign nevi and malignant melanoma. This was proven in large cohorts using tissue microarrays for both HMB45 and NEDD9. While this is novel information that may be useful in further analysis of these tumor types, there is very little diagnostic challenge in differentiating benign nevi from melanoma using standard methods of pathologic evaluation. The real diagnostic dilemma to pathologists lies in the differentiation of benign atypical Spitz nevi from malignant melanoma with Spitzoid features.

A frequent criticism of TMAs is representation of a heterogeneous tumor. 0.6mm cores are only a snap shot of a full section tumor used by pathologists for diagnostic evaluation. It has been shown however that whole section and TMA studies have excellent levels of concordance particularly with redundancy of 2 or greater cores per sample even in heterogeneous tumors such a prostate carcinoma and Hodgkin's lymphoma [28]. In addition, TMAs allow for conservation of limited human tumor tissue in pathology archives.

We moved to whole sections for analysis of Spitz nevi, Atypical Spitz nevi and Spitzoid melanoma. There are four reasons for this. First, there is no TMA currently available for Spitzoid neoplasms due to their scarcity. Second, there are no concordance studies comparing whole section analysis and TMA analysis in Spitz tumors. Third, there is the potential for variable biomarker expression related to location in the epidermal,

junctional or dermal component of the tumor, and a tumor core of 0.6 mm could theoretically not include all three components. Finally, we wanted to mirror what pathologists use in clinical practice. In order to diagnose tumors of melanocytes, pathologists use whole sections.

Our analysis of Nedd9 and HMB45 on TMAs did not hold up to whole section analysis of Spitz tumors. They did not show a differential level of expression according subcellular AQUA ratio of benign Spitz nevi, atypical Spitz nevi and Spitzoid melanoma. This suggests that these biomarkers, analyzed in this fashion, are not useful in differentiating between benign and malignant Spitz tumor types.

What did prove of interest on discovery analysis of the cohort was that the maximum score of HMB45 of a high-powered (20X) field showed differential expression between benign Spitz tumors (typical and atypical) and melanoma with Spitzoid features. This would suggest that concentration of gp100 detected by HMB45 in melanoma is greater than what is encountered in benign Spitz nevi, whether atypical or typical. A focus of very high (quantified by AQUA) HMB45 staining in a Spitz tumor could be of important diagnostic utility. This was represented by the associated ROC curve (Figure 21). While ideally, the ROC would be >0.8 area under the curve, 0.711 is a promising area under the curve for a single biomarker in a small cohort. Future analysis on an independent cohort is necessary for validation.

This analysis is the first set of experiments made possible by the Yale Spitzoid Neoplasm Repository organized and managed by Dr. Rossitza Lasova. The repository includes primary lesions and material from subsequent biopsies from Spitz tumors

collected from the United States and around the world. Tumor samples are paired with relevant clinical data to allow association between histopathologic criteria of the tumor and clinico-pathologic features of the patient. The Spitz neoplasm cohort analyzed here is particularly valuable as the atypical Spitz nevi and Spitzoid melanoma represent equivocal diagnosis. Biomarker profiles that differentiate between benign and malignant tumors would therefore be of particular clinical application should they be able to live up to this rigorous level of testing.

Selected References

1. Fitzpatrick TB, Szabo G. The melanocyte: cytology and cytochemistry. J Invest Dermatol 1959;32:197-209.

2. Rosdahl I, Rorsman H. An estimate of the melanocyte mass in humans. J Invest Dermatol 1983;81:278-81.

3. Szabo G. The number of melanocytes in human epidermis. Br Med J 1954;1:1016-7.

4. Medrano EE, Farooqui JZ, Boissy RE, Boissy YL, Akadiri B, Nordlund JJ. Chronic growth stimulation of human adult melanocytes by inflammatory mediators in vitro: implications for nevus formation and initial steps in melanocyte oncogenesis. Proc Natl Acad Sci U S A 1993;90:1790-4.

5. Kittler H. The Life of Melanocytic Nevi. In: Hans Peter Soyer GA, Rainer Hofmann-Wellenhof and Robert H. Johr, ed. Color Atlas of Melanocytic Lesions of the Skin. Berlin: Springer Berlin Heidelberg; 2007:61-5.

6. Walton RG. Pigmented nevi. Pediatr Clin North Am 1971;18:897-923.

7. Tsao H, Bevona C, Goggins W, Quinn T. The transformation rate of moles (melanocytic nevi) into cutaneous melanoma: a population-based estimate. Arch Dermatol 2003;139:282-8.

8. Chung C, Forte AJ, Narayan D, Persing J. Giant nevi: a review. J Craniofac Surg 2006;17:1210-5.

9. ACS. Cancer facts and figures 2008. In. Atlanta: American Cancer Society; 2008.

10. Spitz S. Melanomas of childhood. Am J Pathol 1948;24:591-609.

11. Sulit DJ, Guardiano RA, Krivda S. Classic and atypical Spitz nevi: review of the literature. Cutis 2007;79:141-6.

12. Herreid PA, Shapiro PE. Age distribution of Spitz nevus vs malignant melanoma. Arch Dermatol 1996;132:352-3.

13. Dahlstrom JE, Scolyer RA, Thompson JF, Jain S. Spitz naevus: diagnostic problems and their management implications. Pathology 2004;36:452-7.

14. Crotty KA, Scolyer RA, Li L, Palmer AA, Wang L, McCarthy SW. Spitz naevus versus Spitzoid melanoma: when and how can they be distinguished? Pathology 2002;34:6-12.

15. Barnhill RL, Flotte TJ, Fleischli M, Perez-Atayde A. Cutaneous melanoma and atypical Spitz tumors in childhood. Cancer 1995;76:1833-45.

16. Spatz A, Ruiter D, Hardmeier T, et al. Melanoma in childhood: an EORTC-MCG multicenter study on the clinico-pathological aspects. Int J Cancer 1996;68:317-24.

17. Wechsler J, Bastuji-Garin S, Spatz A, et al. Reliability of the histopathologic diagnosis of malignant melanoma in childhood. Arch Dermatol 2002;138:625-8.

18. Troxel DB. Medicolegal aspects of error in pathology. Arch Pathol Lab Med 2006;130:617-9.

19. Smoller BR, Hsu A, Krueger J. HMB-45 monoclonal antibody recognizes an inducible and reversible melanocyte cytoplasmic protein. J Cutan Pathol 1991;18:315-22.

20. Rothberg BE, Moeder CB, Kluger H, et al. Nuclear to non-nuclear Pmel17/gp100 expression (HMB45 staining) as a discriminator between benign and malignant melanocytic lesions. Mod Pathol 2008;21:1121-9.

21. Hoashi T, Muller J, Vieira WD, et al. The repeat domain of the melanosomal matrix protein PMEL17/GP100 is required for the formation of organellar fibers. J Biol Chem 2006;281:21198-208.

22. Wick MR, Swanson PE, Rocamora A. Recognition of malignant melanoma by monoclonal antibody HMB-45. An immunohistochemical study of 200 paraffin-embedded cutaneous tumors. J Cutan Pathol 1988;15:201-7.

23. Smoller BR, McNutt NS, Hsu A. HMB-45 staining of dysplastic nevi. Support for a spectrum of progression toward melanoma. Am J Surg Pathol 1989;13:680-4.

24. Bergman R, Dromi R, Trau H, Cohen I, Lichtig C. The pattern of HMB-45 antibody staining in compound Spitz nevi. Am J Dermatopathol 1995;17:542-6.

25. Kim M, Gans JD, Nogueira C, et al. Comparative oncogenomics identifies NEDD9 as a melanoma metastasis gene. Cell 2006;125:1269-81.

26. Natarajan M, Stewart JE, Golemis EA, et al. HEF1 is a necessary and specific downstream effector of FAK that promotes the migration of glioblastoma cells. Oncogene 2006;25:1721-32.

27. Ji H, Ramsey MR, Hayes DN, et al. LKB1 modulates lung cancer differentiation and metastasis. Nature 2007;448:807-10.

28. Giltnane JM, Rimm DL. Technology insight: Identification of biomarkers with tissue microarray technology. Nat Clin Pract Oncol 2004;1:104-11.

29. Camp RL, Chung GG, Rimm DL. Automated subcellular localization and quantification of protein expression in tissue microarrays. Nat Med 2002;8:1323-7.

30. Kallioniemi OP, Wagner U, Kononen J, Sauter G. Tissue microarray technology for high-throughput molecular profiling of cancer. Hum Mol Genet 2001;10:657-62.

31. Pozner-Moulis S, Pappas DJ, Rimm DL. Met, the hepatocyte growth factor receptor, localizes to the nucleus in cells at low density. Cancer Res 2006;66:7976-82.

32. Berger A. Molecular Classification and Prediction of Metastatic Potential in Early Malignant Melanoma:
Discovery and Validation of Biomarkers in the Prognosis of Early Malignant Melanoma. New Haven: Yale University; 2005.